Chemical Engineering Journal 454 (2023) 140194

Contents lists available at ScienceDirect

Chemical Engineering Journal

journal homepage: www.elsevier.com/locate/cej

Review

Advanced ammonium salt materials for electrochemical energy storage: Recent progress and future perspectives

Wanying Zheng [a], Xi Hu [a], Mengcheng Wu [a], Feiyang Zhan [a], Qingqing He [a], Lingyun Chen [a,*], Shaowei Chen [b,*]

[a] Department of Applied Chemistry, School of Chemistry and Chemical Engineering, Chongqing University, Chongqing 401331, PR China
[b] Department of Chemistry and Biochemistry, University of California, Santa Cruz, 1156 High Street, CA 95060, USA

ARTICLE INFO

Keywords:
Ammonium salts
Layered structure
Composites
Supercapacitors
Metal-ion batteries

ABSTRACT

The development of new high-performance materials is essential for robust electrochemical energy storage (EES). In recent years, ammonium salt materials, as an emerging class of layered materials, have attracted considerable attention as electrode materials for EES due to their abundant resources, simple synthesis, low cost, and high specific capacity. This review aims to comprehensively summarize the recent progress of ammonium salt materials for EES. Firstly, the crystal structures and preparation methods of typical ammonium salts including ammonium vanadate, ammonium metal phosphate, and ammonium metal molybdate are discussed. Subsequently, their application for supercapacitors (SCs) and various metal-ion batteries including monovalent alkali ion (Li^+, Na^+, and K^+), ammonium ion (NH_4^+) batteries, zinc ion (Zn^{2+}) batteries, and multivalent alkali-earth ion (Mg^{2+} and Ca^{2+}) batteries is thoroughly introduced. Likewise, the structure–activity relationships between the layered structure of ammonium salts and their electrochemical performance are clarified. In particular, diverse modification strategies including composites, defect, and doping engineering for ammonium salt materials as electrode materials for Zn-ion batteries are presented. Thereafter, various advanced characterization techniques together with theoretical calculations are expounded to further explain the internal structure evolution and reaction mechanism of ammonium salt materials for EES. Finally, a short conclusion and outlook, along with the current challenges and future opportunities of ammonium salts for EES, are proposed.

1. Introduction

Along with the massive consumption of non-renewable fossil fuels and the excessive environmental burden, there is an urgent need to develop efficient electrochemical energy storage (EES) devices with both high energy and power density to store sustainable and clean energy [1–3]. Among various EES systems, supercapacitors (SCs) and rechargeable batteries are considered to be more ideal energy storage devices [4,5]. However, SCs usually suffer from low energy density and high cost while batteries are unsafe and have short cycle life, which greatly limit their large-scale applications [6]. Therefore, researchers have invested a lot of efforts into exploring new high-performance electrode materials to significantly improve the electrochemical performance of both.

It is common knowledge that ideal electrode materials should possess high specific surface area, excellent electrical conductivity, wide operating voltage window, and good structural stability, which are beneficial to provide more electroactive sites, rapidly transport electrons and ions, and avoid the collapse of the material structure [7]. At present, the common electrode materials for SCs and batteries mainly include carbon-based materials, transition metal oxides, transition metal phosphides, and so forth [8]. Among them, transition metal oxides and metal phosphates are considered as promising electrode materials due to their simple synthesis, low cost, and large capacity, and have been extensively

Abbreviations: EES, electrochemical energy storage; SCs, supercapacitors; EDLCs, electricaldouble-layercapacitors; PCs, pseudocapacitors; LIBs, lithium ion batteries; ZIBs, Zn-ion batteries; MIBs, Mg-ion batteries; KIBs, K-ion batteries; CIBs, Ca-ion batteries; AIBs, Ammonium-ion batteries; SIBs, Sodium-ion batteries; AMPs, ammonium transition metal phosphate monohydrate; DFT, discrete fourier transform; 2D, two-dimensional; CNTs, carbon nanotubes; rGO, reduced graphene oxide; NVO, ammonium vanadium oxide; PEDOT, poly(3,4-ethylenedioxythiophene); PVA, polyvinyl alcohol; SCE, saturated calomel electrode; LiPF6, lithium-hexafluoro phosphate; KPF6, potassium-hexafluoro phosphate.

* Corresponding authors.
E-mail addresses: lychen@cqu.edu.cn (L. Chen), shaowei@ucsc.edu (S. Chen).

https://doi.org/10.1016/j.cej.2022.140194
Received 28 July 2022; Received in revised form 15 October 2022; Accepted 31 October 2022
Available online 4 November 2022

researched [9,10]. More particularly, vanadium oxides have attracted much attention because of their multivalent (from +2 to +5) and thus wide potential windows [11]. However, vanadium oxides encounter the bottleneck of low electrical conductivity and poor cycling stability. Subsequently, metal cations such as Zn^{2+} [12], Na^{+} [13], and K^{+} [14] with large ionic radius and high atomic weight have been introduced as pillars to stabilize the structure and expand the ion diffusion channels, but their specific capacity is limited by the high molar mass [15]. With this context, ammonium vanadate formed by intercalating NH_4^+ pillars with lower atomic mass between vanadium oxide layers can provide higher storage capacity, which makes ammonium salt material a potential candidate as promising electrode materials [16]. Based on many research studies, the addition of NH_4^+ to form ammonium vanadate as an electrode material may be an advisable choice to improve the electrochemical performance of SCs and batteries, which has the following specific advantages [17]: (i) NH_4^+ ions can achieve a pillar effect by intercalating into each vanadium-oxide layer, which can prevent a structural collapse caused by the ion insertion/extraction during the charge–discharge process [18]. (ii) A network of strong N—H···O hydrogen bonds among NH_4^+ ions and vanadium-oxide layers can vastly improve the structural stability, playing a special role in enhancing the electrode material's cycling stability [19]. (iii) NH_4^+ with a large ionic radius (143 pm) can offer large interlayer distance, contributing to the enhanced ion diffusion rate [20,21]. (iv) Compared to the common intercalation metal ions, NH_4^+ with the lower density as well as molecular weight can provide higher specific gravimetric and volumetric capacities theoretically [22]. As early as 1995, Carling et al. reported a series of ammonium metal phosphate monohydrate ($NH_4M^{II}PO_4\ H_2O$, M^{II} = Mn, Fe, Co, and Ni) and revealed the crystal structure, which consisted of approximately square-planar layers of highly distorted $M^{II}O_6$ corner-sharing octahedra linked to regular PO_4^{3-} and NH_4^+ tetrahedra via hydrogen bonds [23]. More importantly, metal-water interactions (*i.e.* $M^{2+}\cdots H_2O$ and $NH_4^+\cdots H_2O$) and highly efficient electroactive sites in $NH_4M^{II}PO_4\ H_2O$ can be conducive to fast ion and electron transport together with high redox-active centres, which are crucial for energy storage processes [7]. Additionally, ammonium molybdate with the advantage of industrial low cost in ammonium salt materials has also gradually emerged recently, becoming a potential participant in electrode materials [24,25]. NH_4^+ ions are connected to the structural layers of ammonium molybdate and play a role in stabilizing the structure and balancing charges [26].

Structural property is one of the most significant properties of electrode materials, which determines the physical and chemical properties of materials [27]. In terms of the performance of SCs and batteries, it largely depends on the electrode materials, and therefore, the development of novel electrode materials with unique structural features is the key to enhance the overall performance of EES devices [28]. Thereinto, ammonium salt materials, an emerging class of materials with a unique layered structure, have exhibited excellent electrochemical performance and great potential for energy storage [29]. The novel layered crystal structure of ammonium salt materials can offer the following advantages: (i) The layered structure can provide great channels for the diffusion of ions and electrolytes, and be propitious to ion intercalation/extraction [27,30]. (ii) Also, the layered structure offers a high specific surface area, sufficient electroactive sites and high theoretical charge storage capacity so that it can accommodate fairly large number of ions

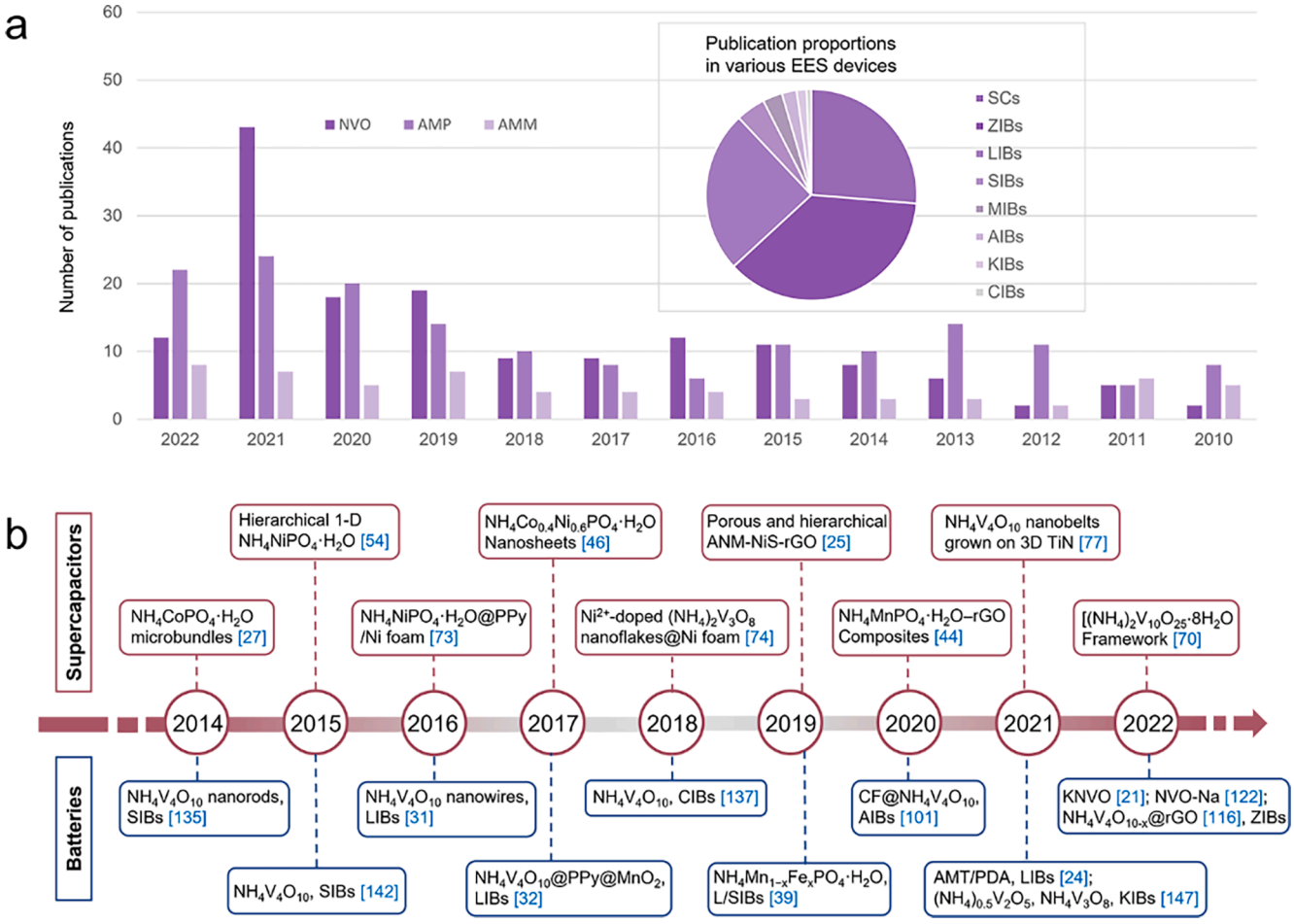

Fig. 1. (a) Publication numbers and proportions of typical ammonium salt materials for EES in recent years. (b) Application progress of typical ammonium salt materials and their composites in the field of energy storage.

[31]. (iii) ammonium salt materials with layered structure can be easier combined with other active materials to form composite materials, which can synergistically improve their performance [32]. Taking into account all the above advantages of ammonium salt materials, they have been gradually applied in the fields of energy storage in recent years (Fig. 1a). Nevertheless, there are still some defects in practical applications of ammonium salt materials, such as limited electronic conductivity and low discharge capacity at high current density [33]. In order to solve these problems, researchers put forward several modification strategies including compounding with active materials [25,34], doping elements [16], and introducing defect ions [35], *etc*.

To date, there are few reviews on ammonium salt materials as a new class of materials, and some are only a brief overview of a certain ammonium salt. For example, Li et al. reviewed the recent progress of metal (Co and Ni) phosphate based materials for high-performance SCs, of which ammonium/bimetallic phosphates were only mentioned as a small part [9]. In addition, Raju focused on the energy storage applications of ammonium metal phosphates in SCs and rechargeable batteries. However, other ammonium salt materials such as ammonium vanadate or ammonium molybdate have not been reviewed yet [7]. Fig. 1b depicts some key developments of typical ammonium salt materials for SCs and batteries. Yet up to now, there is no systematic review of ammonium salt materials used in the field of energy storage. Considering the growing attention of ammonium salt materials and the breakthrough progress in EES applications in recent years, it is very necessary to conduct a thorough and comprehensive review of this emerging field, which provides reference and direction for researchers to further explore the new field of ammonium salts in the future.

Herein, we review the recent progress of ammonium salt materials in EES field. Firstly, we introduce the crystal structures of representative ammonium salts (*i.e.* ammonium vanadate, ammonium metal phosphate and ammonium molybdate). Then, we discuss the common synthetic methods including hydrothermal/solvothermal, microwave, and other methods. After that, we focus on the application progress of ammonium salt materials in SCs and various metal-ion batteries. Furthermore, advanced characterization techniques and theoretical calculation methods are elaborated, which aims to further understand the relationship between the internal structure evolution and electrochemical mechanism. Finally, the current challenges and perspectives of ammonium salt materials in EES devices are summarized.

2. Crystal structure of typical ammonium salts

Crystal structure determines the properties of materials to a great extent. No matter ammonium vanadate, ammonium metal phosphate or ammonium metal molybdate, they all have a layered structure, in which the interlayer NH_4^+ can act as a pillar to stabilize the layered structure, thus ensuring the long-term cycling stability of ammonium salts as electrode materials.

2.1. Ammonium vanadate

Ammonium vanadate, with the general formula of $(NH_4)_xV_yO_z$ (abbreviated as NVO or AVO), is generally characterized by a layered structure. The layered structure of NVO is usually composed of VO_5 square pyramids and VO_6 octahedra or/and VO_4 tetrahedra [36]. The NH_4^+ ions are placed between the vanadium-oxide layers, forming a network of N—H···O hydrogen bonds between the cationic and anionic layers, which act as "pillars" to stabilize the layered structure [37]. Benefiting from the advantages of the layered structure, when NVO is used as an electrode material for batteries, this structure can provide two-dimensional interstitial spaces for guest ions and achieve high specific capacity [38].

Taking $NH_4V_3O_8$ as an example, as shown in Fig. 2a, the layered

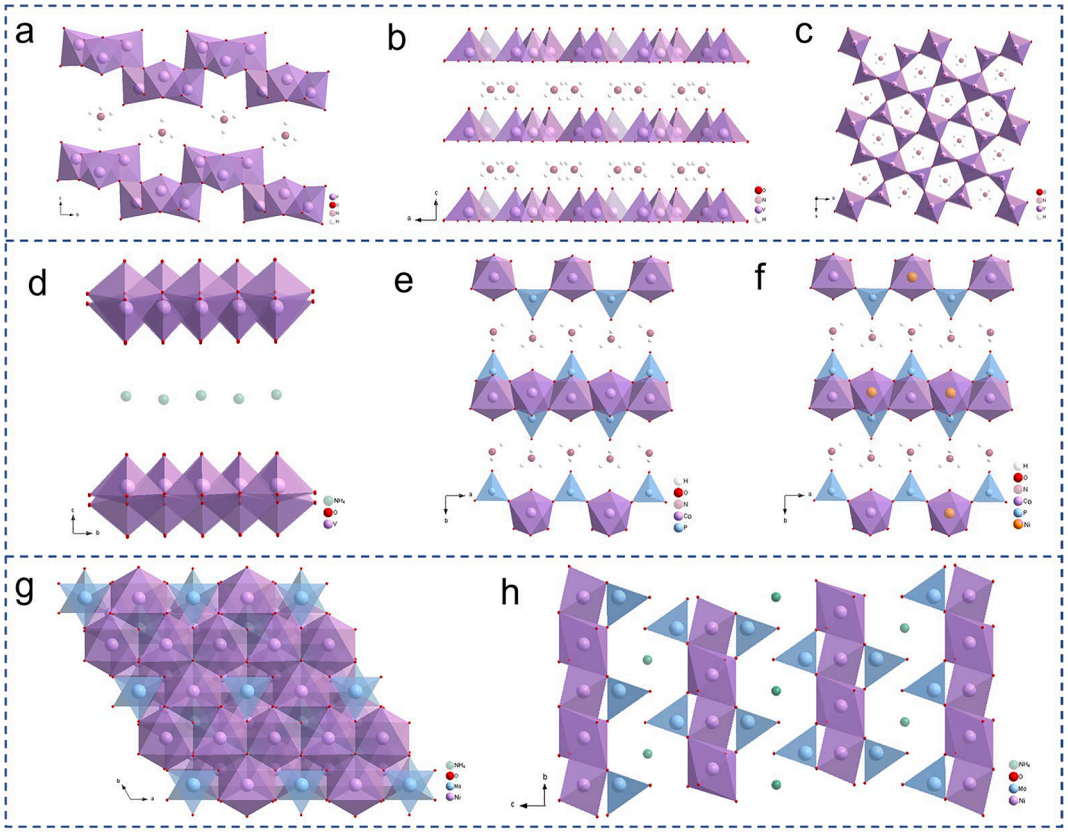

Fig. 2. The crystal structure of (a) $NH_4V_3O_8$, $(NH_4)_2V_3O_8$ viewed along the (b) *b* and (c) *c* axes, (d) $NH_4V_4O_{10}$, (e) $NH_4CoPO_4\ H_2O$, (f) $NH_4Co_{0.33}Ni_{0.67}PO_4\ H_2O$, $(NH_4)HNi_2(OH)_2(MoO_4)_2$ viewed along the (g) *c* and (h) *a* axes.

structure is formed by distorted VO_5 square pyramids and VO_6 octahedra, in which pairs of square pyramids sharing edges form double zigzag chains along the *b*-axis, with VO_6 octahedra located between these chains. Each octahedron shares vertices and edges with two bi-square pyramids in adjacent chains. In addition, from the Fig. 2b and c, we can see that $(NH_4)_2V_3O_8$ possesses a two-dimensional structure that consists of VO_5 square pyramids and corner-sharing VO_4 tetrahedra, where each V^{4+} ion has six nearest neighboring magnetic ions. The 2D morphology and hydrogen bonds between VO_x layers are regarded as two critical factors for maintaining structural stability during ion intercalation/deintercalation. Similar in structure to $(NH_4)_2V_3O_8$, $NH_4V_4O_{10}$ is composed of a warped zigzag configuration parallel to the (0 0 l) plane shapes of VO_5 square pyramid units and skewed VO_6 octahedrons (Fig. 2d) [17].

2.2. Ammonium phosphate

Among the ammonium phosphate materials, the most studied is the ammonium transition metal phosphate monohydrate ($NH_4M^{II}PO_4\ H_2O$, M^{II} = Mn, Fe, Co, Ni), whose general formula is AMPs, which belongs to the dittmarite family and has a unique layered structure with open-framework [7,39]. AMP compounds were said to crystallize in the orthorhombic $Pmn2_1$ space group. The structure of AMPs consisted of approximately square-planar layers of highly distorted $M^{II}O_6$ corner-sharing octahedra (the point symmetry being C_{2v}) linked to regular PO_4^{3-} and NH_4^+ tetrahedra via hydrogen bonds [23].

Taking $NH_4CoPO_4\ H_2O$ as an example, the structure is formed from sheets of distorted CoO_6 corner-sharing octahedra bridged through the oxygen atoms of the phosphate tetrahedra (Fig. 2e) [29]. These layers are interconnected by hydrogen bonds with the NH_4^+ cations inserted between the sheets. $NH_4MnPO_4\ H_2O$, a new modification of niahite, crystallizes in the space group P*nam* with cell parameters $a = 17.582$ Å, $b = 4.909$ Å and $c = 5.731$ Å, where a unit cell parameter is twice that of the mineral structure [40]. Importantly, metal-water interactions (*i.e.* $M^{2+}\cdots H_2O$ and $NH_4^+\cdots H_2O$) and highly efficient electroactive sites in AMPs can be used for fast ion and electron transport, which are crucial for energy storage processes [7]. As displayed in Fig. 2f, the crystal structure of $NH_4Co_{0.33}Ni_{0.67}PO_4\ H_2O$ suggested that NH_4^+ interacted in the interlayer of the P—O–Ni polyhedron, allowing it to undergo rapid ion exchange with surrounding cations in the electrolyte [41].

2.3. Ammonium molybdate

Ammonium metal molybdate, abbreviated as AMM (where M in the middle stands for transition metal), is a class of ammonium molybdate whose crystal structure has been studied more, usually in a layered structure. For example, layered ammonium nickel molybdate $(NH_4)HNi_2(OH)_2(MoO_4)_2$ is triangular with hexagonal unit cell parameters $a = 6.0147(4)$ Å, $c = 21.8812(13)$ Å, and $Z = 3$ [42]. As shown in Fig. 2g and h, the structure consists of 2D layers of twisted nickel octahedra that share edges to form layers perpendicular to the *c*-axis. Molybdate tetrahedra are bound to nickel octahedra through shared MoO–Ni bonds, and these tetrahedral molybdate groups are then stacked together to form a 3D layered structure through strong hydrogen-bonding interactions [25]. Each unit cell has three layers with ammonium ions bound between the layers to balance the charge. In addition, layered ammonium zinc molybdate $(NH_4)HZn_2(OH)_2(MoO_4)_2$ also has the same crystal structure with hexagonal unit-cell parameters of a = 6.10767(15) Å and c = 21.6409(6) Å [26].

3. Synthetic methods of ammonium salt materials

The successful synthesis of ammonium salt materials with controllable morphology plays a crucial role in the subsequent study of their structure and electrochemical properties. Due to its potential huge application prospects, various methods have been developed to prepare ammonium salt materials, the most common of which are hydrothermal/solvothermal method [43], but also microwave method [44], precipitation method [45], and others [46].

3.1. Hydrothermal method

Hydrothermal method is one of the most universal techniques to obtain micro- and nanosized ammonium salt materials. And hydrothermal treatment can reliably control the composition and morphology of the products, and is currently the most efficient method to synthesize nanocomposites [47].

Traditional hydrothermal method refers to a chemical reaction carried out in a sealed pressure vessel with an aqueous solution as the solvent at a certain temperature, time, and pH. For example, $NH_4V_3O_7$ has been synthesized by a conventionally simple hydrothermal method using NH_4VO_3 and citric acid as raw materials at 180 °C for 1 or 2 days [47]. As for AMPs, a unique interface-rich core–shell ammonium nickel cobalt phosphate (NCoNiP@NCoNiP) has been constructed through a facile two-step hydrothermal route [48]. To improve the electrochemical performance of pristine $NH_4(Ni,Co)PO_4\ H_2O$, Ma et al. [49] successfully used the hydrothermal approach to prepare $NH_4(Ni,Co)PO_4\ H_2O$/CFs composite (Fig. 3a), which made the ions more mobile because of the synergistic effect between $NH_4(Ni,Co)PO_4\ H_2O$ and conductive CFs. As a member of the ammonium salt family, ammonium metal molybdate is mostly prepared by hydrothermal method. For instance, both $(NH_4)[Fe(MoO_4)_2]$ and $(NH_4)HNi_2(OH)_2(MoO_4)_2$ (ANM) have been synthesized with $(NH_4)_6Mo_7O_{24}\ 6H_2O$ as a part of the precursor under hydrothermal treatment [50]. Inspired by the fact that ANM is a good precursor for unsupported hydrodesulfurization catalysts, Ke et al. [25] synthesized ANM-NiS-rGO ternary composite using $NiCl_2\ 6H_2O$, thiourea and ammonia as raw materials under the premise of synthesis MoO_2-rGO by hydrothermal method at 180 °C for 12 h.

3.2. Solvothermal method

Solvothermal method is developed on the basis of hydrothermal method. Different from hydrothermal method, solvothermal method is carried out with organic solvents (such as ethanol, ethylene glycol (EG), glycerol, SDBS, *etc.*) as the reaction medium [51–53]. The microdendrites of $NH_4NiPO_4\ H_2O$ (ANP_{md}), microplatelets (ANP_{mp}) and microrods (ANP_{mr}) were prepared in EG, water, and EG/water mixture through facile solvothermal processes, respectively [54]. Therefore, the manipulation of reaction conditions is crucial for the control of material morphology. Layered $NH_4Co_xNi_{1-x}PO_4\ H_2O$ ($0 < x < 1$) nanostructures with different Co/Ni molar ratios were obtained via a solvothermal method and verified by electrochemical test that the sample with a Co/Ni ratio of 2/3 showed the best electrochemical performance [29]. Accidentally, Jiang and coworkers [55] observed the spontaneous knitting behavior of ultrathin $(NH_4)_{0.38}V_2O_5$ nanoribbons/CNTs (NVO/CNTs) through a solvothermal treatment (Fig. 3b).

Even though hydrothermal and solvothermal synthesis are the most common methods to obtain ammonium salt materials, there are still essential shortcomings to be overcome. Hydrothermal and solvothermal reaction systems are in a closed container, so it is not convenient to visually detect the progress of the reaction, only the results can be seen, and it is difficult to adjust the reaction parameters and study its mechanism, which is not conducive to the synthesis of perfect crystals of ammonium salt materials.

3.3. Microwave method

Microwave method is a method that uses microwaves as a heating tool to achieve stirring at the molecular level and overcome the disadvantage of uneven heating of the hydrothermal container. Compared with the hydrothermal method, the microwave method has a higher reaction rate due to the higher heating rate of the system, and thus

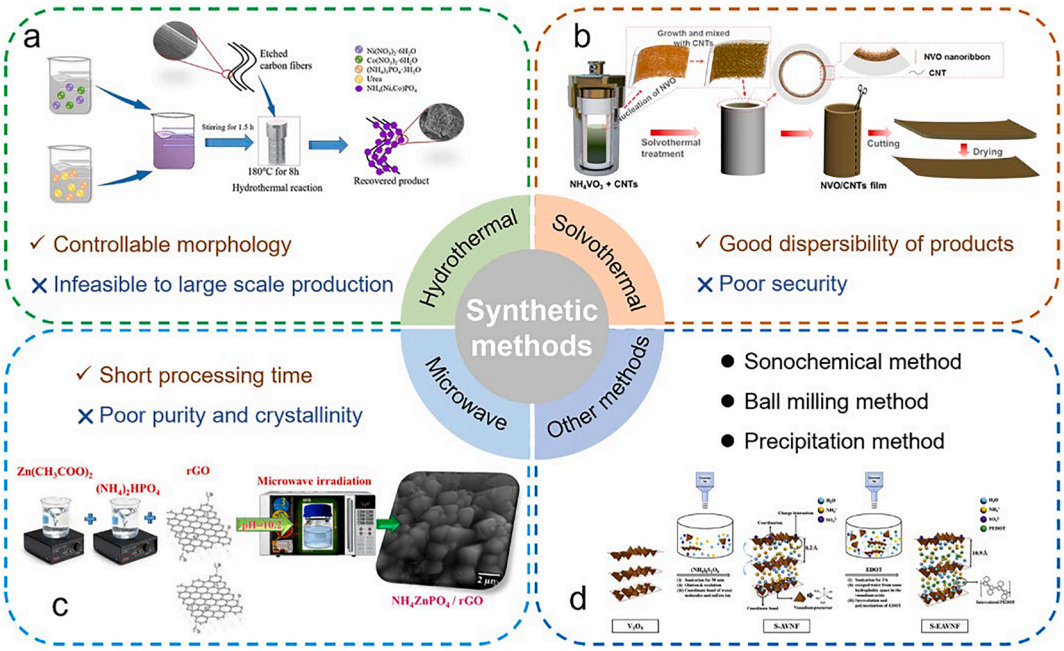

Fig. 3. Synthetic methods and corresponding advantages and disadvantages for ammonium salt materials. (a) Synthesis steps of $NH_4(Ni,Co)PO_4$/CFs composite materials. (a) Reproduced with permission [49]. Copyright 2022, Wiley-VCH. (b) Schematic illustration of the spontaneous knitting process of ultrathin NVO nanoribbons/CNTs. (b) Reproduced with permission [55]. Copyright 2021, Elsevier. (c) Synthesis of NH_4ZnPO_4/rGO composite. (c) Reproduced with permission [59]. Copyright 2019, Wiley-VCH. (d) Schematic diagram of the intercalation of PEDOT and ammonium cations into vanadate layers and coordination of sulfate ions during the fabrication of nanofiber composites by the sonochemical method. (d) Reproduced with permission [61]. Copyright 2019, Elsevier.

significantly shortens the reaction time [56]. Microwave method can obtain ammonium salts with different structures and morphologies by changing the reaction conditions [57]. For instance, $NH_4V_3O_8$ materials with controlled shape and morphology (flower, nanobelt, lath and sheet structures) by simply controlling pH value were produced by microwave hydrothermal method [58]. For AMPs, various polymorphs of 2D NH_4MnPO_4 H_2O have been obtained by microwave irradiation and hydro/solvothermal processes using ethylene glycol (EG), H_2O (W), and EG/W mixed solvents as the reaction medium with the use of different surfactants [4]. Raja et al. synthesized NH_4ZnPO_4/rGO [59] (Fig. 3c) and NH_4MnPO_4 H_2O-rGO [44] successively by microwave route.

Although the above methods are extensively used to prepare ammonium salt materials, the synthesis conditions are harsh and the purity of the synthesized materials is low. Therefore, in order to make up for the shortcomings of the above methods, it is necessary to develop some other new synthetic methods.

3.4. Other methods

Other methods such as reflux method, sonochemical method, mechanical ball milling method, precipitation method, *etc.* have been used to synthesize ammonium salt materials. For ammonium vanadate nanofiber ($(NH_4)_2V_6O_{16}$ $1.5H_2O$) (AVNF), Lee's group [60] prepared poly(3,4-ethylenedioxythiophene) (PEDOT) intercalated AVNF (E-AVNF) using reflux method, in which PEDOT exhibited good electrical conductivity and electrochemical behavior. However, reflow method required a long reaction time (16 h) and formed irregular interplanar spacing distances when PEDOT intercalated, which was not conducive to the intercalation/de-intercalation of electrolyte K^+ ions [61]. Thus, they switched to a simple and effective sonochemical method to synthesize E-AVNF composites (S-EAVNF) in a very short time (3 h) (Fig. 3d), which overcame the above problems [61]. Additionally, some researchers have developed wet mechanical ball milling method to prepare AMPs. For example, Kozawa's group [62] used ball milling method to prepare NH_4CoPO_4 H_2O platelets, which was formed by the repeating dissolution–recrystallization reactions during the milling process. Pang and coworkers [63] synthesized NH_4CoPO_4 H_2O with various morphologies (oblong plate, microplate, microflower, hierarchical architectures) by a simple chemical precipitation approach without surfactants and templates. In one earlier study [64], amorphous Co-Ni pyrophosphates with controllable Co^{2+}/Ni^{2+} ratio were fabricated from the mixture of $NiSO_4$ $6H_2O$, $CoSO_4$ $7H_2O$ and $(NH_4)_3PO_4$ $3H_2O$ via a co-precipitation process at 140 °C for 12 h.

This section summarizes several common methods for synthesizing ammonium salt materials, all with their own advantages and disadvantages. Although hydro/solvothermal method synthesizes materials with controlled morphology and high purity, its equipment requirements are high. Conversely, the microwave method requires low reaction conditions and has fast reaction speed, but low product purity. Combining it with the hydrothermal method can quickly obtain high-purity materials, greatly improving production efficiency and expanding the scope of practical applications. In addition, the sol–gel method can realize complete and accurate control of the reaction process, which just makes up for the uncontrollable shortcoming of hydro/solvothermal process. More importantly, the sol–gel method prepares materials with a wide range of doping, accurate stoichiometry and easy modification, which is conducive to the production of materials with better performance and is expected to be used in the synthesis of ammonium salt materials.

4. Applications of ammonium salt materials for EES

4.1. Applications of ammonium salt materials for SCs

SCs, as one of the most promising energy storage devices, have attracted tremendous attention because of their high power density (500–10,000 W kg^{-1}) and long cycle life (>10^6 cycles) [65,66]. Based on charge storage mechanism, SCs can be divided into two categories: one is electrical double-layer capacitors (EDLCs) that store energy through surface-controlled ion adsorption; the other is pseudocapacitors (PCs) based on faradaic processes involving fast surface/near-surface redox reactions [67]. Obviously, PCs undergo redox reactions that can

store more charges to increase capacitance, which exactly can compensate for the low energy density (1–10 Wh kg^{-1}) of SCs. Furthermore, developing high-performance active electrode materials is essential to obtain SCs with high energy density and large specific capacitance [4]. As a new type of popular material, ammonium salt materials especially AMPs are extensively used in SCs due to the addition of NH_4^+ which makes their high theoretical specific capacitance, excellent electrical conductivity and long-term cycle stability (Table 1).

4.1.1. Ammonium monometallic phosphates

As a class of efficient electrode materials, AMPs (NH_4MPO_4 H_2O, M = Ni^{2+}, Co^{2+}, Mn^{2+}, and Fe^{2+}) exhibit rapid electron and ion transport, which can mainly be attributed to their more electroactive sites and higher redox-active centres, thereby significantly improving its electrochemical performance [7]. In other words, the control of structure and morphology has an obvious effect on the capacitance behavior of electrode materials. For instance, Pang and coworkers [63] synthesized various NH_4CoPO_4 H_2O nano/microstructures with the use of different ammonium solvents. NH_4CoPO_4 H_2O hierarchical architectures demonstrated excellent specific capacitance of 369.4 F g^{-1} at 0.625 A g^{-1}. However, NH_4CoPO_4 H_2O hierarchical architectures still suffer from poor cycle stability. To overcome this problem, they firstly developed unique layered NH_4CoPO_4 H_2O microbundles that compose of 1D layered microrods, which remained 92.7 % of its initial specific capacitance after 3000 cycles [27].

Besides, it is worth noting that the dimensional control of the materials and the adjustment of its surface parameters also play an important role in improving the electrochemical performance. On this basis, Raju and coworkers [4] synthesized NH_4MnPO_4 H_2O (AMP) and further exfoliated with the aid of ultrasonicaction for 15 min in the water–acetone mixture to obtain exfoliated 2D nanosheets (denoted AMP-P-15 min) to assemble symmetric supercapacitor (Fig. 4a), which alleviated the phenomenon of nanosheets stacking. From the SEM images (Fig. 4b), the 2D nanosheets of NH_4MnPO_4 H_2O with the width of about 200 nm and highly desirable surface facets of (0 1 0) obtained by using PVP as a surfactant. After testing, whether AMP-P-15 min is used for symmetry or asymmetric devices, it exhibits excellent rate performance. The symmetric supercapacitor device of AMP-P-15 min showed a surprising gravimetric capacitance of 48.4 F g^{-1} at 5 mV s^{-1} and maintained a capacitance of 38.8 F g^{-1} even at 100 mV s^{-1}. Also, the asymmetric device constructed with AMP-P-15 min delivered an extraordinary cycle stability with capacity attenuation by ~7 % after 100 k cycles (Fig. 4c).

4.1.2. Ammonium bimetallic phosphates

Ammonium bimetallic phosphates (AMM'Ps) have also attracted much attention from researchers. In particular, ammonium cobalt–nickel phosphate can significantly improve the electrochemical performance of electrode materials due to the strong synergistic effect between cobalt and nickel, making it have the potential for wide application in the field of electrochemical energy storage [68]. Take the study of Chen et al. [69] as an example, they assembled the hybrid capacitor (NH_4-Co-Ni phosphate (NCNP)//HPC) constructed with NCNP as positive electrode and the hierarchical porous carbon (HPC) as negative electrode in 6 M KOH electrolyte solution delivers a high energy density of 29.6 Wh kg^{-1} equivalent to a power density of 11 kW kg^{-1}.

Furthermore, the adjustment of the molar ratios of cobalt and nickel of NCNP is also worthy of our consideration. Proved by electrochemical tests, $NH_4Co_xNi_{1-x}PO_4$ H_2O with a Co/Ni ratio of 2:3 characterized by layered nanoplate structure and rich uniform pores displayed the highest specific capacitance (1567 F g^{-1} at 1 A g^{-1}) [29]. On the basis of this research, Li et al. [46] adopted liquid-phase exfoliated technique to synthesize $NH_4Co_{0.4}Ni_{0.6}PO_4$ H_2O nanosheets with the exfoliation solvent of formamide solution under ultrasonication for 4 days (Fig. 4d and e), which can effectively improve the electronic conductivity of materials. The asymmetric device AC//$NH_4Co_{0.4}Ni_{0.6}PO_4$ H_2O nanosheets showed outstanding cycle stability (retaining 102.3 % of specific capacitance even after 10,000 GCD cycles at 2 A g^{-1}, presented in Fig. 4f).

4.1.3. Ammonium salt composites

Nowadays, the ammonium salt composite electrode has gradually attracted the attention of researchers, which can make up for their shortcomings such as poor electronic conductivity and combine their advantages to a certain extent. In 2021, Wang et al. [70] assembled a flexible quasi-solid-state hybrid supercapacitor with NVO@CFF cathode and AC@CFF anode by using NH_4Cl/polyvinyl alcohol (PVA) gel electrolyte. The HSC device displayed excellent stability over 12,000 cycles with more than 67 % capacitance retention, in which NH_4Cl/PVA electrolyte played an important role in improving the storage performance of NH_4^+.

Additionally, graphene that often used as a conductive network is an interesting choice to increase the electrical conductivity. Badr et al. [71]

Table 1
Summary of electrochemical performances of typital ammonium salt materials for SCs.

Materials	Morphology	Electrolyte	Potential window	Specific capacitance (current density scan rate^{-1})	Cycling stability (cycles, current density)	Ref.
$NH_4CoPO_4{\cdot}H_2O$	Hierarchical architecture	3 M KOH	0–0.6 V vs SCE	369.4 F g^{-1} (0.625 A g^{-1})	99.7 % (400, 0.625 A g^{-1})	[63]
$NH_4CoPO_4{\cdot}H_2O$	Microbundle	3 M KOH	0–0.5 V vs SCE	662 F g^{-1} (1.5 A g^{-1})	92.7 % (3000, 1.5 A g^{-1})	[27]
$NH_4NiPO_4{\cdot}H_2O$	Microrod	3 M KOH	0–0.5 V vs Ag/AgCl	545 F g^{-1} (10 A g^{-1})	~80 % (5000, 10 A g^{-1})	[54]
$NH_4MnPO_4{\cdot}H_2O$	Nanosheet	3 M KOH	0–0.5 V vs Ag/AgCl	423 F g^{-1} (5 mV s^{-1})	97 % (10,000, 1 A g^{-1})	[4]
$(NH_4)(Ni,Co)PO_4{\cdot}0.67H_2O$	Hierarchical structure	6 M KOH	0–0.5 V vs SCE	1297 F g^{-1} (0.5 A g^{-1})	—	[69]
$NH_4Co_xNi_{1-x}PO_4{\cdot}H_2O$ (Co/Ni 2:3)	Layered nanostructure	3 M KOH	0–0.5 V vs SCE	1567 F g^{-1} (1 A g^{-1})	97.6 % (3000, 15 A g^{-1})	[29]
$NH_4Co_{0.4}Ni_{0.6}PO_4{\cdot}H_2O$	Nanosheet	3 M KOH	0–0.6 V vs SCE	820 F g^{-1} (1 A g^{-1})	—	[46]
Ni(Co)NH_4PO_4@rGO	Microplate	6 M KOH	0–0.4 V vs Ag/AgCl	1020 F g^{-1} (1 A g^{-1})	125 % (5000, 10 A g^{-1})	[72]
$NH_4MnPO_4{\cdot}H_2O$-rGO (GO 50 mg)	Hierarchical structure	2 M H_2SO_4	0–1.0 V vs Ag/AgCl	705 F g^{-1} (1 A g^{-1})	85.9 % (5000, 20 A g^{-1})	[44]
NVO	—	1 M NH_4Cl/PVA	−0.8–1.0 V vs Ag/AgCl	339 F g^{-1} (0.5 A g^{-1})	71 % (14,000, 0.5 A g^{-1})	[70]
S-EAVNF	Nanofiber	2 M KCl	0–0.9 V vs SCE	202 F g^{-1} (3 mV s^{-1})	—	[61]

Note: rGO, reduced graphene oxide; NVO, ammonium vanadium oxide; S-EAVNF, PEDOT-intercalated ammonium vanadate nanofiber composites by sonochemical method; PEDOT, poly(3,4-ethylenedioxythiophene); PVA, polyvinyl alcohol; SCE, saturated calomel electrode.

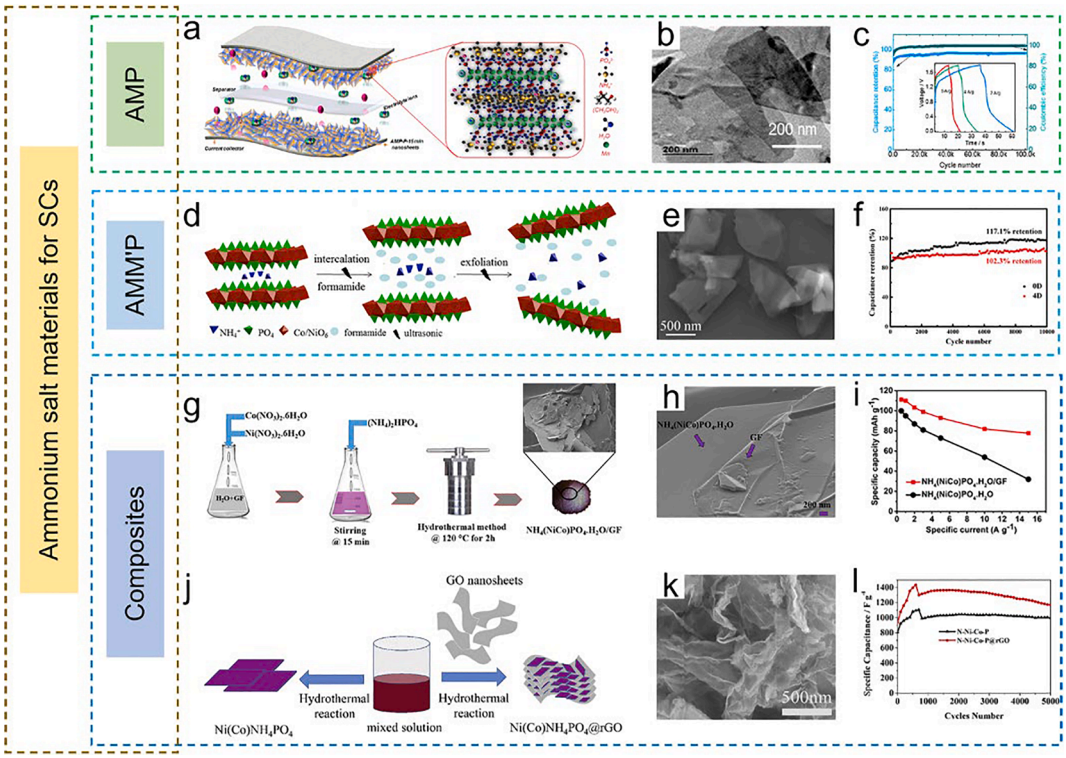

Fig. 4. Ammonium salt materials for SCs. (a) Schematic illustration of the working principle of a symmetric supercapacitor device constructed with exfoliated AMP-P nanosheets in an aqueous electrolyte of 3 M KOH. (b) SEM image of exfoliated nanosheets of AMP-P-15 min. (c) Cycle stability test employed at a current density of 5 A g^{-1} for about 100 k consecutive cycles; the inset shows the charge–discharge plots obtained at current densities of 2, 4, and 5 A g^{-1}. (a–c) Reproduced with permission [4]. Copyright 2019, American Chemical Society. (d) Schematic illustration of the crystal structure and the exfoliation process, and (e) SEM image of $NH_4Co_{0.4}Ni_{0.6}PO_4$ H_2O. (f) Cycling life at a current density of 2 A g^{-1} (10,000 cycles). (d–f) Reproduced with permission [46]. Copyright 2017, Elsevier. (g) Synthesis route and (h) SEM image of $NH_4(NiCo)PO_4$ H_2O/GF composites. (i) Specific capacity of $NH_4(NiCo)PO_4{\cdot}H_2O$ and $NH_4(NiCo)PO_4$ H_2O/GF at (0.5–15 A g^{-1}) specific currents calculated from GCDs. (g–i) Reproduced with permission [71]. Copyright 2021, Elsevier. (j) Schematic illustration of the fabrication of $Ni(Co)NH_4PO_4$ and $Ni(Co)NH_4PO_4$@rGO. (k) SEM image of $Ni(Co)NH_4PO_4$@rGO. (l) Cycling performance at current density of 10 A g^{-1} of $Ni(Co)NH_4PO_4$ and $Ni(Co)NH_4PO_4$@rGO. (j–l) Reproduced with permission [72]. Copyright 2018, Elsevier.

synthesized $NH_4(NiCo)PO_4$ H_2O/GF composites via a hydrothermal route (Fig. 4g and h), whose specific capacity (111 mAh g^{-1}) is higher than that of $Ni(NH_4)_2(PO_3)_4$ $4H_2O$/60 mg GF (52.7 mAh g^{-1}) they prepared before (Fig. 4i), which may be ascribed to the synergistic effect of nickel and cobalt. Meanwhile, reduced graphene oxide (rGO) is also a popular conductive material. In 2018, Zhang et al. [72] produced a type of rGO-modified Ni-Co phosphates ($Ni(Co)NH_4PO_4$@rGO) microplates (Fig. 4j and k). Benefiting from the incorporation of rGO, the obtained $Ni(Co)NH_4PO_4$@rGO as electrodes for supercapacitors showed a higher specific capacitance (1020F g^{-1} at 1 A g^{-1}) compared with $Ni(Co)NH_4PO_4$ without rGO (877 F g^{-1}). Particularly, the cycling stability of this composite material can retain 125 % after 5000 GCD cycles (Fig. 4l), indicating the great potential for practical applications. Modifying with graphene to improve the properties of materials can also be applied to ammonium metal molybdate materials. Ke et al. [25] firstly prepared a unique ternary composite ANM-NiS-rGO with 3D porous flower-like structures. It imparted high specific capacity of 56 mAh g^{-1} at 2 A g^{-1} because of the synergistic effects of the ternary composite.

In order to effectively improve the conductivity of ammonium salt materials, researchers have also made some other efforts such as conductive polymer modification [61,73], heteroatom doping engineering [74], acting as conductive electrolyte [75,76] and others [77]. For example, Lee et al. [61] prepared PEDOT-intercalated ammonium vanadate nanofiber (S-EAVNF) for pseudocapacitors. The composite renders a high surface area of 85.5 m^2 g^{-1} and excellent electrical conductivity of 4.1 × 10^{-2} S cm^{-1} due to the intercalation of PEDOT, which can improve the electrical conductivity and expand the interlayer distance of the lattice of vanadate nanofibers. Meanwhile, the S-EAVNF electrodes exhibited fast kinetics and pseudocapacitive properties, and the reversible electrochemical redox reactions can be expressed as follows:

$$(NH_4)_2V_6O_{16} + xK^+ + xe^- \leftrightarrow K_x(NH_4)_2V_6O_{16} \quad (1)$$

During K^+ ion intercalation/deintercalation process into host, the valence state of V changes between +4 and +5. Thus, the corresponding theoretical capacity of $(NH_4)_2V_6O_{16}$ is 269 mAh g^{-1}.

Although AMPs has been reported as a potential candidate for energy storage devices (especially SCs), the accessibility of electrons and ions to all electroactive sites is still a challenge and also suffer from limited electronic conductivity. Therefore, there are still critical issues related to the structure–property relationship to be solved. Adding conductive additives to AMPs is the key to obtain high electronic conductivity. Meanwhile, more attractive performances of NVOs and AMMs need to be further developed in the future research work to meet the energy storage requirements of SCs.

4.2. *Applications of ammonium salt materials for batteries*

Batteries store charge involving transformation of chemical bonds through diffusion-controlled faradaic redox reactions in the bulk of active materials, which have the higher energy density (~300 Wh kg^{-1} of Li-ion batteries) but lower power density (<1000 W kg^{-1}) and shorter life (~1000 cycles) compared with SCs [67]. To break through these limitations, researchers have devoted themselves to developing electrode materials with layered structure, large specific surface area and excellent electrical conductivity to meet people's needs for high-

performance batteries [6]. Ammonium salt materials, especially NVOs, have been widely studied as electrode materials for batteries due to their simple synthesis, low cost, high capacity and stable structure (as summarized in Table 2).

4.2.1. Li-ion batteries

Nowadays, rechargeable lithium ion batteries (LIBs) possess the advantages of high energy density, long cycle life, and excellent rate performance that have attracted tremendous attention [78]. Nevertheless, it is found that LIBs still suffer from some defects such as low power density, the lack of lithium resources and safety issues, which are huge obstacles for its longterm development [6]. As a consequence, it is critical to develop the LIBs with excellent performance in capacity, power and energy density, and safety. Recently, researchers have made some attempts to use ammonium salt materials as electrode materials for LIBs, and the results show that this approach has achieved certain effects. Generally speaking, NH_4^+ ions between the layered ammonium salts can not only achieve the pillar effect to prevent the structure collapse caused by the intercalation/extraction of Li^+ during the charge-discharge process, but also increase the interlayer spacing to accommodate fairly large number of Li^+ ions and promote their migration. Therefore, ammonium salt family can exhibit high rate performance and good cyclic stability, which makes it a promising electrode material for LIBs.

4.2.1.1. $NH_4V_3O_8$. Tremendous attention has been focused on $NH_4V_3O_8$ and their composites as cathode materials for LIBs due to their remarkable electrochemical properties, such as high capacity, good capacity retention and long cycle life.

To the best of our knowledge, the morphology determines the performance of the materials to a certain extent. For example, Wang et al. [79] incorporated CNTs into $NH_4V_3O_8$ flakes ($NH_4V_3O_8$/0.5 wt% CNTs composites) to improve the electronic conductivity, which shows a high discharge capacity up to 358.7 mAh g^{-1} at 0.03 A g^{-1}. Then, one-dimensional $NH_4V_3O_8$ $0.37H_2O$ nanorods were also reported by their team [80] with high electrochemical performance via SDBS assisted hydrothermal method for LIBs, which delivered a maximum specific discharge capacity of 327.1 mAh g^{-1} at 0.03 A g^{-1}.

In order to obtain better electrochemical properties and facilitate the practical applications of $NH_4V_3O_8$ cathodes, many researchers make much more efforts on the nanostructural control. For instance, Kou's team [53] used NH_4VO_3 and polyethylene glycol (PEG-4000) as reactants at different pH to prepare self-assembled cactus-like $NH_4V_3O_8$ (Fig. 5a). The electrochemical measurements indicate that the sample with pH value of 3.7 delivers higher discharge capacity compared to the other samples, attributing to the cactus structure with robust structural stability during cycling. It can be seen that adjusting the pH value of the solution can effectively control the morphology of $NH_4V_3O_8$, which can also be confirmed by Cheng et al. [58], who synthesized $NH_4V_3O_8$ flower, nanobelt, lath and sheet by controlling pH value. Among all of the structure, the $NH_4V_3O_8$ nanobelt exhibited best electrochemical performance, presenting the first discharge capacity of 328 mAh g^{-1} and a superior rate capacity of 208 mAh g^{-1} at 0.3 A g^{-1} (Fig. 5b). Besides, Kou and coworkers successfully fabricated rGO/$NH_4V_3O_8$ composites [10] to overcome the limitation of low-electronic conductivity and long lithium ion diffusion path of $NH_4V_3O_8$, which significantly improved the electrochemical property for $NH_4V_3O_8$ cathode materials of LIBs.

4.2.1.2. $NH_4V_4O_{10}$. $NH_4V_4O_{10}$ also attracts much attention of researchers, whose structure is similar to $NH_4V_3O_8$ materials, in which the NH_4^+ ions are intercalated between two bilayer of V_2O_5, resulting higher electronic conductivity and fast lithium diffusion in comparison with V_2O_5 cathode [81]. Hence $NH_4V_4O_{10}$ and its composites are the potential electrode materials with a high electrochemical performance [17,18,31,32,82–84]. For instance, Zhang et al. [82] have reported the synthesis of $NH_4V_4O_{10}$ nanobelts with an initial discharge capacity of 171.8 mAh g^{-1} at 0.125 A g^{-1} and similarly Wang et al. [83] have prepared $(NH_4)_{0.5}V_2O_5$ nanobelts with the first discharge capacity of 225.2 mAh g^{-1} at 0.015 A g^{-1}. We found that the results of the electrochemical performance of $(NH_4)_{0.5}V_2O_5$ nanobelts can only be measured at low current power, restricting the material for high power applications. In order to breakthrough this barrier, Sarkar et al. [84] studied the impact of binder on stable high rate electrochemical performance of $NH_4V_4O_{10}$ and it was found that carboxy methyl cellulose (CMC) based cathode delivers superior capacity (200 mAh g^{-1} at 1 A g^{-1}).

To further enhance the capacity, cyclic stability, and rate capability of $NH_4V_4O_{10}$, Wang et al. [32] fabricated a unique hierarchical $NH_4V_4O_{10}$@ PPy@MnO_2 nanowire arrays as electrode materials for LIBs (Fig. 5c). After electrochemical testing, $NH_4V_4O_{10}$-PPy-MnO_2 nanowires exhibited higher capacitance than that of the simple $NH_4V_4O_{10}$-PPy core@shell or $NH_4V_4O_{10}$ nanowires (Fig. 5d), which can be attributed to the synergistic effect of ternary materials. As far as we know, the 3D nanostructure materials can not only avoid the disadvantages of low-dimensional nanomaterials such as poor cycling and rate performances which were caused by their serious self-aggregations, but also can preserve their advantages with good specific capacity [85]. Liu et al. [18] proposed a β-cyclodextrin (β-CD)-assisted hydrothermal method to prepare mesoporous $NH_4V_4O_{10}$ nanoflowers composed of nanoflakes as cathode materials for LIBs. The nanoflowers showed specific capacity retains 103.5 mAh g^{-1} after 200 cycles even at 1 A g^{-1}.

4.2.1.3. Other ammonium vanadates. Apart from $NH_4V_3O_8$ and $NH_4V_4O_{10}$, a new type of ammonium vanadium bronze, $(NH_4)_2V_7O_{16}$ [86,87], is also an attractive electrode material, whose layered structure is similar to other vanadium bronzes but with an unprecedented stoichiometry and crystal structure, enabling the intercalation of various guest ions (Fig. 5e). When intercalating lithium ions into $(NH_4)_2V_7O_{16}$, it shows an initial discharge capacity of 232 mAh g^{-1} and an average discharge voltage of 2 V (vs Li/Li^+) (Fig. 5f and g).

To the best of our knowledge, not only temperature and pH can affect the morphology and properties of ammonium vanadates, but pressure is also a non-negligible factor in the synthesis process, which is first demonstrated by the study of Sadowska et al [88]. They used a simple hydrothermal method with different initial pressure values (0, 5, 25, and 50 bar) to prepare $(NH_4)_2V_6O_{16}$ and $(NH_4)_2V_{10}O_{25}$ $8H_2O$ with different morphologies and found that the pure $(NH_4)_2V_{10}O_{25}$ $8H_2O$ could be obtained at a pressure of 50 bar and revealed its excellent behavior as cathode material for LIBs. The theoretical capacity of $(NH_4)_2V_{10}O_{25}$ $8H_2O$ is at least 221 mAh g^{-1} when not less than $9Li^+$ ions are inserted in theory.

Studies have shown that bi or multi-cations vanadium bronzes such as ammonium and sodium bi-cation vanadium bronze [33,89] can effectively promote the electrochemical performance of materials. Fei et al. [89] fabricated 3D flower-like $(NH_4)_{0.83}Na_{0.43}V_4O_{10}$ $0.26H_2O$ vanadium bronze nano-platelet clusters. This material exhibited good cycle stability at different discharge rates (0.18–0.67 C rate) and voltage limits (1.5–3.4 V and 2.0–3.4 V). Similarly, Fei and coworkers [33] developed sodium intercalated $(NH_4)_2V_6O_{16}$ in the same way. It's not hard to prove that ammonium sodium vanadium bronze has smaller charge transfer resistance than ammonium vanadium bronze, which would favor superior discharge capacity and rate performance.

4.2.1.4. Other ammonium salt materials. As we know, AMP is widely used as electrode material for SCs, but AMP and AMM are mostly used as precursors for the synthesis of other metal salts [62,90], therefore few works directly apply them as electrode material for LIBs. However, due to the unique layered structure of these materials [91], some researchers still insist on exploring the preparation methods to develop their application in LIBs. For example, Chen et al. [8] exploited solid-state

Table 2
Summary of electrochemical performances of typital ammonium salt materials for batteries.

Materials	Morphology	Applications	Electrolyte	Voltage range	Specific capacity (current density)	Cycling stability (cycles, current density)	Ref.
$NH_4V_3O_8$/0.5 wt% CNTs	Flake-like	LIBs	1 M $LiPF_6$ in EC/DMC	1.5–4.0 V vs Li/Li^+	358.7 mAh g^{-1} (0.03 A g^{-1})	97 % (100, 0.15 A g^{-1})	[79]
$(NH_4)_{0.5}V_2O_5$	Nanobelt	LIBs	1 M $LiPF_6$ in EC/DMC	1.8–4.0 V vs Li/Li^+	225.2 mAh g^{-1} (0.015 A g^{-1})	81.9 % (100, 0.15 A g^{-1})	[83]
$NH_4V_4O_{10}$	Nanoflower	LIBs	1 M $LiPF_6$ in EC/PC/DMC	2.0–4.0 V vs Li/Li^+	242.8 mAh g^{-1} (0.2 A g^{-1})	64.9 % (200, 1 A g^{-1})	[18]
$NH_4V_4O_{10}$	Nanowire	LIBs	1 M $LiPF_6$ in EC/DMC	2.0–4.0 V vs Li/Li^+	205 mAh g^{-1} (0.05 A g^{-1})	—	[31]
$(NH_4)_2V_7O_{16}$	Layered structure	LIBs	1 M $LiPF_6$ in EC/DMC	1.3–3.2 V vs Li/Li^+	232 mAh g^{-1} (0.01 A g^{-1})	84 % (50, 0.02 A g^{-1})	[86]
$NH_4MnPO_4{\cdot}H_2O$	Lumpy particle	LIBs	1 M $LiPF_6$ in EC/DEC	0.01–3.0 V vs Li/Li^+	222.1 mAh g^{-1} (0.05 A g^{-1})	—	[8]
AMT/PDA	Flake	LIBs	1 M $LiPF_6$ in EC/DEC	0.005–2.5 V vs Li/Li^+	1471 mAh g^{-1} (0.1 A g^{-1})	—	[24]
$NH_4V_3O_8{\cdot}1.9H_2O$	Nanobelt	ZIBs	3 M $Zn(CF_3SO_3)_2$	0.2–1.4 V vs Zn/Zn^{2+}	463 mAh g^{-1} (0.1 A g^{-1})	81 % (2000, 10 A g^{-1})	[93]
$NH_4V_4O_{10}$	Lamellar structure	ZIBs	3 M $Zn(CF_3SO_3)_2$	0.8–1.7 V vs Zn/Zn^{2+}	147 mAh g^{-1} (0.2 A g^{-1})	70.3 % (5000, 5 A g^{-1})	[103]
$NH_4V_4O_{10}$	Decussate structure	ZIBs	3 M $Zn(CF_3SO_3)_2$	0.1–1.6 V vs Zn/Zn^{2+}	417.35 mAh g^{-1} (0.1 A g^{-1})	90 % (2100, 5 A g^{-1})	[107]
$(NH_4)_2V_{10}O_{25}{\cdot}8H_2O$	Nanobelt	ZIBs	3 M $Zn(CF_3SO_3)_2$	0.7–1.7 V vs Zn/Zn^{2+}	229.5 mAh g^{-1} (0.1 A g^{-1})	90.1 % (5000, 5 A g^{-1})	[108]
$(NH_4)_2V_3O_8$/C	Nanoparticle	ZIBs	3 M $Zn(CF_3SO_3)_2$	0.4–1.6 V vs Zn/Zn^{2+}	356 mAh g^{-1} (0.1 A g^{-1})	—	[112]
NV NSs@ACC	Nanosheet	ZIBs	3 M $Zn(CF_3SO_3)_2$	0.4–1.4 V vs Zn/Zn^{2+}	523 mAh g^{-1} (0.1 A g^{-1})	~85 % (1000, 2 A g^{-1})	[111]
NVO@CF	Nanoflake	ZIBs	2 M $ZnSO_4$	0.2–1.4 V vs Zn/Zn^{2+}	434 mAh g^{-1} (0.5 A g^{-1})	83 % (2500, 20 A g^{-1})	[113]
$(NH_4)_{0.38}V_2O_5$/CNTs	Nanoribbon	ZIBs	2 M $ZnSO_4$	0.2–1.5 V vs Zn/Zn^{2+}	465 mAh g^{-1} (0.1 A g^{-1})	89.3 % (500, 0.1 A g^{-1})	[55]
NHVO@$Ti_3C_2T_x$	Hybrid film	ZIBs	3 M $Zn(CF_3SO_3)_2$	0.2–1.2 V vs Zn/Zn^{2+}	514.7 mAh g^{-1} (0.1 A g^{-1})	84.2 % (6000, 5 A g^{-1})	[34]
O_d-NVO-SS-2	Cistern-like nanobelt	ZIBs	3 M $Zn(CF_3SO_3)_2$	0.4–1.6 V vs Zn/Zn^{2+}	331.4 mAh g^{-1} (0.3 A g^{-1})	—	[119]
ZNV	Microsphere	ZIBs	3 M $Zn(CF_3SO_3)_2$	0.2–1.8 V vs Zn/Zn^{2+}	461.1 mAh g^{-1} (0.1 A g^{-1})	> 90 % (3500, 2 A g^{-1})	[35]
Ti-doped $NH_4V_4O_{10}$	Nanobelt	ZIBs	3 M $Zn(CF_3SO_3)_2$	0.5–1.7 V vs Zn/Zn^{2+}	263 mAh g^{-1} (0.1 A g^{-1})	89.02 % (2000, 2 A g^{-1})	[16]
MVO-0.1	Nanowire	ZIBs	1 M $Zn(OTF)_2$	0.4–1.4 V vs Zn/Zn^{2+}	337 mAh g^{-1} (0.1 A g^{-1})	83.6 % (500, 0.5 A g^{-1})	[125]
KNVO	Nanobelt	ZIBs	3 M $Zn(CF_3SO_3)_2$	0.2–1.6 V vs Zn/Zn^{2+}	464 mAh g^{-1} (0.1 A g^{-1})	90 % (3000, 5 A g^{-1})	[21]
$(NH_4)_2V_6O_{16}{\cdot}1.5H_2O$	Nanowire	ZIBs	3 M $Zn(CF_3SO_3)_2$	0.4–1.6 V vs Zn/Zn^{2+}	385 mAh g^{-1} (0.1 A g^{-1})	75 % (10,000, 8 A g^{-1})	[126]
$NH_4V_4O_{10}{\cdot}0.28H_2O$	Microflower	ZIBs	2 M $Zn(CF_3SO_3)_2$	0.2–1.6 V vs Zn/Zn^{2+}	410 mAh g^{-1} (0.2 A g^{-1})	76 % (500, 2 A g^{-1})	[106]
PEDOT-NVO	Connected nanobelt	ZIBs	3 M $Zn(CF_3SO_3)_2$	0.4–1.6 V vs Zn/Zn^{2+}	356.8 mAh g^{-1} (0.05 A g^{-1})	94.1 % (5000, 10 A g^{-1})	[130]
$NH_4V_4O_{10}$	Nano-belt	SIBs	1 M $NaClO_4$ in EC/PC	1.5–3.5 V vs Na/Na^+	190 mAh g^{-1} (0.2 A g^{-1})	80 % (50, 0.5 A g^{-1})	[142]
$NH_4V_4O_{10}$	Nanorod	SIBs	1 M $NaClO_4$ in PC	1.5–3.4 V vs Na/Na^+	175.7 mAh g^{-1} (0.02 A g^{-1})	—	[135]
$NH_4V_4O_{10}$	Nanobelt	SIBs	1 M $NaClO_4$ in PC	0.01–3.0 V vs Na/Na^+	148 mAh g^{-1} (1 C)	—	[139]
K-NVG	Nanosheet clusters	SIBs	1 M $NaClO_4$ in EC/EMC/DMC	0.05–3.0 V vs Na/Na^+	235.4 mAh g^{-1} (0.1 A g^{-1})	82 % (250, 0.3 A g^{-1})	[143]
$NH_4V_4O_{10}$	Nanobelt	MIBs	0.5 M $Mg(ClO_4)_2$ in AN	−0.6–1.0 V vs Mg/Mg^{2+}	174.8 mAh g^{-1} (0.2 C)	—	[144]
$NH_4V_4O_{10}$	Micro-flower	MIBs	1 M LiCl in 0.4 M APC	0.5–2.0 V vs Mg/Mg^{2+}	228 mAh g^{-1} (0.1 A g^{-1})	75 % (100, 0.1 A g^{-1})	[30]
$NH_4V_4O_{10}$	Flower-like	KIBs	0.8 M KPF_6 in EC/PC	1.0–4.2 V vs K/K^+	136 mAh g^{-1} (0.05 A g^{-1})	90 % (200, 3 A g^{-1})	[136]
$(NH_4)_{0.5}V_2O_5$	Nanowire	KIBs	1.5 M KFSI in EC/DEC	1.5–3.8 V vs K/K^+	97.8 mAh g^{-1} (0.025 A g^{-1})	—	[147]
NVO@SDBS	Uniform rod-like	CIBs	$Ca(ClO_4)_2$ xH_2O in CH_3CN	−0.6–1.3 V vs Ag/Ag^+	150 mAh g^{-1} (0.1 A g^{-1})	—	[137]
CF@$NH_4V_4O_{10}$	Urchin-like	AIBs	1 M $(NH_4)_2SO_4$	0–1.0 V vs Ag/AgCl	143 mAh g^{-1} (0.1 A g^{-1})	82.5 % (100, 0.1 A g^{-1})	[138]
$NH_4V_3O_8{\cdot}2{\cdot}.9H_2O$	Nanobelt	AIBs	1 M $(NH_4)_2SO_4$	0–1.0 V vs Ag/AgCl	121 mAh g^{-1} (0.1 A g^{-1})	95 % (400, 0.1 A g^{-1})	[150]

Note: CNTs, carbon nanotubes; AMT/PDA, $(NH_4)_6Mo_7O_{24}$/polydopamine; NV NSs@ACC, 2D hydrated ammonium vanadate nanosheets (NV NSs) grown on alkali-treated carbon cloth; NVO@CF, $NH_4V_4O_{10}$ nanoflakes grown on carbon fiber (CF); NHVO@$Ti_3C_2T_x$, $(NH_4)_2V_{10}O_{25}$ $8H_2O$@$Ti_3C_2T_x$; O_d-NVO-SS-2, stainless steel (SS) supported oxygen-rich vacancy $(NH_4)_2V_{10}O_{25}$ $8H_2O$ with the mass of glucose 0.2 g; ZNV, cation-deficient $Zn_{0.3}(NH_4)_{0.3}V_4O_{10}$ $0.91H_2O$; MVO-0.1, Mo-doped $NH_4V_4O_{10}$ with $(NH_4)_6Mo_7O_{24}$ 0.1 g; KNVO, potassium ammonium vanadate; PEDOT-NVO, poly(3,4-ethylenedioxythiophene) intercalated $NH_4V_3O_8$; K-NVG, K-

doped $(NH_4)_2V_3O_8$/graphene; NVO@SDBS, $NH_4V_4O_{10}$@sodium dodecylbenzenesulfonate; $LiPF_6$, lithium-hexafluoro phosphate; KPF_6, potassium-hexafluoro phosphate; EC, ethylene carbonate; DMC, dimethyl carbonate; DEC, diethyl carbonate; EMC, ethylmethyl carbonate; PC, propylene carbonate; $Zn(OTF)_2$, Zinc trifluoromethylsulfonate; AN, acetonitrile; APC, aqueous potassium carbonate; KFSI, potassium bis(fluorosulfonyl)-imide.

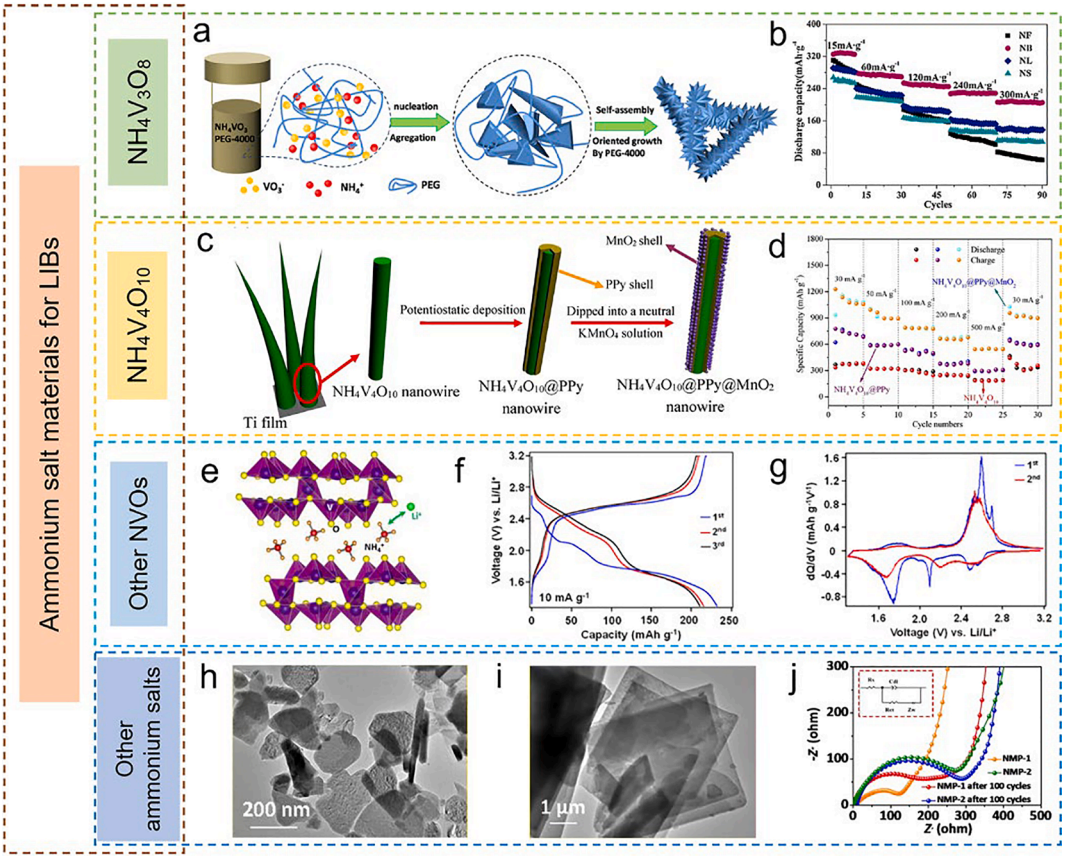

Fig. 5. Ammonium salt materials for LIBs. (a) Schematic illustration of cactus-like $NH_4V_3O_8$ by PEG4000-assisted hydrothermal method. (a) Reproduced with permission [53]. Copyright 2020, Elsevier. (b) Rate capability of the NF, NB, NL and NS. (b) Reproduced with permission [58]. Copyright 2016, Elsevier. (c) Schematic illustration of the fabrication process for $NH_4V_4O_{10}$@PPy@MnO_2 nanowire arrays on Ti film. (d) Rate performances at various current rates from 30 to 500 mA g^{-1} with respect to the cycle numbers. (c, d) Reproduced with permission [32]. Copyright 2017, Elsevier. (e) Schematic diagram of the crystal structure of Li^+ intercalation $(NH_4)_2V_7O_{16}$. (f) Initial three cycles of galvanostatic discharge/charge profiles at 10 mA g^{-1} and (g) its corresponding differential capacity (dQ/dV) plots for the initial two cycles of $(NH_4)_2V_7O_{16}$/Li. (e-g) Reproduced with permission [86]. Copyright 2020, American Chemical Society. TEM images of (h) NMP-1 and (i) NMP-2. (j) Nyquist plots of the NMP-1 and NMP-2 based cells. (h–j) Reproduced with permission [8]. Copyright 2020, Elsevier.

reaction and co-precipitation reaction to design and fabricate lumpy particles (marked as NMP-1) and thin sheets (marked as NMP-2) NH_4MnPO_4 H_2O, respectively (Fig. 5h and i). When used as anode for LIBs, NMP-1 exhibits better electrochemical performance, such as higher discharge capacity of 1307 mAh g^{-1} at 0.1 A g^{-1} after 350 cycles, better cycling stability and lower R_{ct} compared with NMP-2 (Fig. 5j), which can be ascribed to the smaller longitudinal–transverse ratio of lumpy particles and porous structure.

In 2021, Xie et al. [24] demonstrated that $(NH_4)_6Mo_7O_{24}$ (AMT) can not only serve as a precursor for the synthesis of molybdenum-based anode materials for LIBs, but itself can also realize reversible lithium storage. Meanwhile, they also developed recrystallization and freeze drying methods to prepare AMT/polydopamine (PDA) composite to further enhance electrochemical performance. The as-prepared AMT/PDA composite shows flake morphology and delivers a reversible discharge capacity of 702 mAh g^{-1} at 0.3 A g^{-1}.

4.2.2. Zn-ion batteries

Although LIBs have dominated energy storage systems for decades, the problems of their high cost, limited lithium natural resources, and flammable and toxic organic electrolytes are not conducive to sustainable development and hinder their long-term application [92–94]. By contrast, Zn-ion batteries (ZIBs) have captured massive attention recently related with the favorable features including low cost, high natural abundance and high safety, low redox potential (−0.762 V vs SHE) as well as high theoretical capacity (820 mAh g^{-1}, 5855 mAh cm^{-3}) [95,96]. As a result, ZIBs are the most potential alternative batteries for LIBs. Many materials such as MnO_2 [97], Prussian blue analogs [98] and vanadium-based materials [93] have been used as zinc-ion cathode materials. Among them, layered vanadium-based materials have the advantages of low cost, high capacity, and good cycle stability with a stable structure, which make them the promising cathode materials for aqueous ZIBs [99]. Specifically, ammonium vanadate is widely used as a cathode material for ZIBs [100].

4.2.2.1. Pristine ammonium vanadates. To date, a series of vanadium-based materials, especially the emerging ammonium vanadate materials, have become a hot spot for researchers to develop as cathode materials for ZIBs [22,56,101,102].

$NH_4V_4O_{10}$ [103,104], as an important member of the ammonium vanadate family, it has aroused tremendous interest of researchers. For instance, Yang et al. [103] manufactured a bilayered $NH_4V_4O_{10}$ with a self-healing lamellar architecture and tunable interlayer spacing during charge–discharge as cathode material for ZIBs (Fig. 6a and b), which

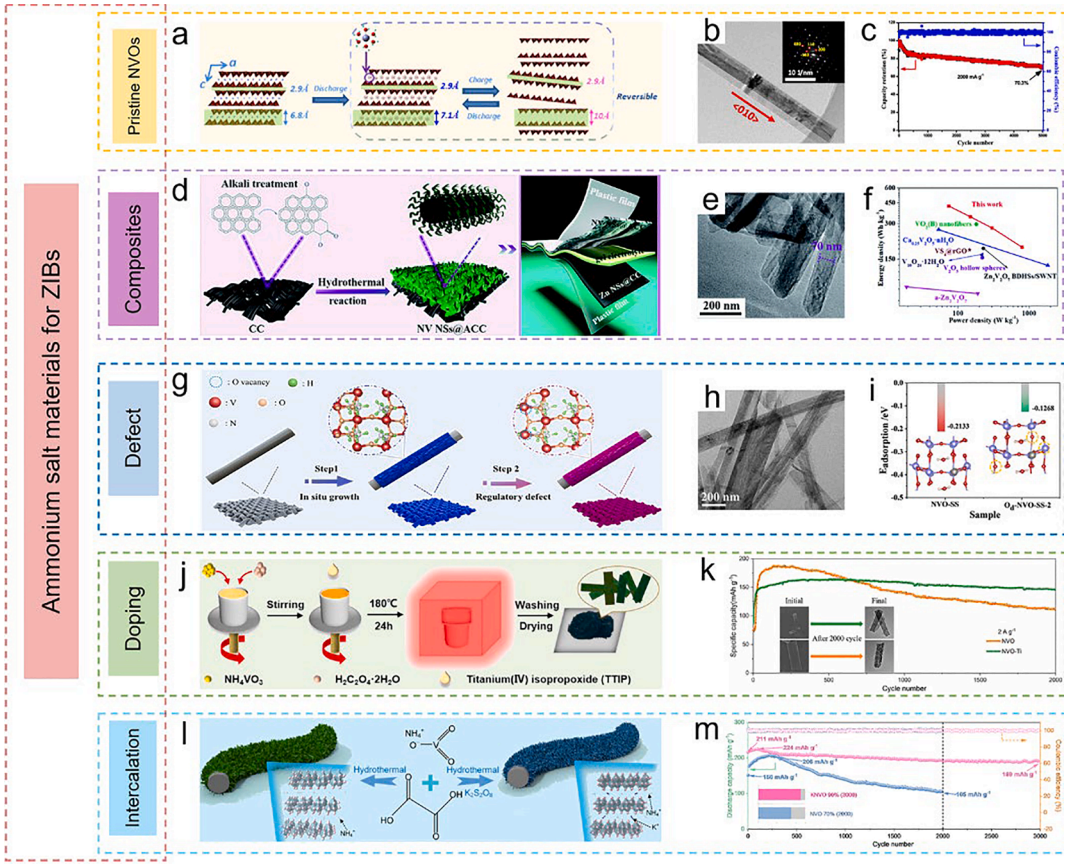

Fig. 6. Ammonium salt materials for ZIBs. (a) Schematic diagram of interlayer spacing adjustment of $NH_4V_4O_{10}$ during reversible charge–discharge process. (b) TEM image of $NH_4V_4O_{10}$. (c) Long-term cycling properties at a current density of 2000 mA g^{-1} of the $NH_4V_4O_{10}$//Zn cell. (a–c) Reproduced with permission [103]. Copyright 2018, American Chemical Society. (d) Schematic illustration of the fabrication procedure for the flexible NV NSs@ACC electrode. (e) TEM image and (f) Ragone plots of NV NSs@ACC. (d–f) Reproduced with permission [111]. Copyright 2020, The Royal Society of Chemistry. (g) Schematic diagram of the synthesis process and (h) TEM image of O_d-NVO-SS-2. (i) The adsorption/desorption of Zn^{2+} on the surface of the O_d-NVO-SS-2 and NVO-SS electrode. (g-i) Reproduced with permission [119]. Copyright 2021, Elsevier. (j) Schematic diagram of preparation process of Ti-doped $NH_4V_4O_{10}$. (k) The long-term cycling performance of at 2 A g^{-1} for NVO and NVO-Ti; the inset is TEM images of morphological changes of NVO-Ti and NVO electrodes after 2000 cycles. (j, k) Reproduced with permission [16]. Copyright 2020, Elsevier. (l) Schematic illustration of the preparation process and the crystal structure, and (m) Cycling performance at 5 A $g^{-1}$of NVO and KNVO. (l, m) Reproduced with permission [21]. Copyright 2022, American Chemical Society.

enables a specific capacity of 147 mAh/g in the voltage window of 0.8–1.7 V vs Zn^{2+}/Zn and a capacity retention of 70.3 % over 5000 cycles at 2 A/g (Fig. 6c). In order to further enhance Zn^{2+} ion intercalation kinetics and long-term cycling stability, researchers make their great efforts to explore 3D $NH_4V_4O_{10}$ for ZIBs [105–107]. Sun and co-workers [107] prepared a novel self-templated $NH_4V_4O_{10}$ with a microsized decussate superstructure. The special decussate morphology consists of giant crossed nanobelts, which is beneficial to enhance the structural stability and further improve the cycling performance, manifesting 221.4 mAh/g after 2100 cycles.

Additionally, Wei et al. [108] synthesized ultrathin $(NH_4)_2V_{10}O_{25}$ $8H_2O$ nanobelts for AZIBs with an energy density of 225.4 Wh kg^{-1} between a wide power density of $10^2 \sim 10^4$ W kg^{-1}, owing to the ultrathin stable structure and the adjustable large interlayer spacing. Subsequently, Cui et al. [109] prepared layer-by-layer stacked $(NH_4)_2V_4O_9$ $0.5H_2O$ nanosheet assemblies and $(NH_4)_2V_4O_9$ nanosheets towards high performance ZIBs, demonstrating $(NH_4)_2V_4O_9$ a promising cathode material for ZIBs.

Ammonium vanadate can be used not only for aqueous zinc-ion batteries, but also as cathode electrode materials for quasi-solid-state zinc-ion batteries. In the study of Chen et al. [110], who assembled a high-concentration salt electrolyte (HCSE) with high-capacity $NH_4V_3O_8$ $1.9H_2O$ cathode and zinc foil anode to form flexible QSS ZIBs, exhibiting a discharge capacity of 283 mAh g^{-1} at 20 °C, 215 mAh g^{-1} at 0 °C, and 119 mAh g^{-1} at −20 °C.

4.2.2.2. Composites. Most of the reported cathode materials suffer from sluggish ion/electron transfer kinetics due to relatively poor electrical conductivity, which limits further applications of the materials [111]. Composites are made by introducing another or more material components with different physical and chemical properties in a designed form, ratio and distribution. The various constituent materials of composites play a synergistic role in performance, with superior comprehensive performance that cannot be matched by a single material. Carbon material can effectively improve the conductivity of materials, and introducing it into ammonium vanadate to form a composite material can overcome the above problems, thereby improving the electrochemical performance.

For instance, $(NH_4)_2V_3O_8$/C was synthesized via a facile one-step hydrothermal process by Jiang et al. [112], who demonstrated that $(NH_4)_2V_3O_8$/C can effectively store Zn^{2+}. And the Zn//$(NH_4)_2V_3O_8$/C battery delivered a high energy density of 334 Wh kg^{-1} at 294 W kg^{-1}. Moreover, given that the use of inactive organic binders (PTFE, PVDF, PP, *etc.*) invisibly increases the dead mass of the cathode, thus limiting the overall energy density of the full devices [111]. Additionally, the increased electrical resistance of the cathode in the battery decreases the capacity, cycling stability and rate capability of the AZIBs [113]. To overcome these limitations, researchers focus on developing ammonium

vanadate on substrates (*e.g.*, CC, CF, and CNTs) as the binder-free cathodes for AZIBs. Jiang et al. [111] used a simple alkali-treated carbon cloth (ACC) as a self-supporting substrate to in-situ grow ultrathin 2D hydrated ammonium vanadate nanosheets (NV NSs) (Fig. 6d and e). The results show that the NV NSs@ACC cathode in coin-typed battery can deliver a high reversible capacity of 523 mAh g^{-1} at 0.1 A g^{-1}, and a remarkable energy density of 343 Wh kg^{-1} at 150 W kg^{-1} (Fig. 6f). Inspired by this, Tamilselvan et al. [113] proposed an ultrathin $NH_4V_4O_{10}$ (NVO) nanoflake grown on pretreated CFs as a flexible binder-free cathode in AZIBs. The electrochemical performance of both cathode materials mentioned above has been improved, which may be attributed to the ultrathin nature of NVO flakes that shortens the diffusion lengths of ions and electrons during charge–discharge cycles. Accidentally, Jiang and coworkers [55] observed the spontaneous knitting behavior of ultrathin $(NH_4)_{0.38}V_2O_5$ nanoribbons/CNTs (NVO/CNTs). This binder-free paper cathode of ZIBs showed high reversible capacities of 465 mAh g^{-1} at 0.1 A g^{-1}, thanks to the enhanced electronic conductivity and rich meshes due to the incorporation of CNTs. Wang et al. [34] reported a novel $(NH_4)_2V_{10}O_{25}$ $8H_2O$@$Ti_3C_2T_x$ (NHVO@$Ti_3C_2T_x$) film anode for constructing "rocking-chair" ZIBs. Benefiting from the advantage of the crystal structure of NHVO and the assistance of $Ti_3C_2T_x$ nanosheets, NHVO@$Ti_3C_2T_x$//$ZnMn_2O_4$ full battery delivers the highest specific capacity of 131.7 mAh g^{-1} at 0.1 A g^{-1} compared to all reported aqueous "rocking-chair" Zn ion full battery.

4.2.2.3. Defect engineering. Defect engineering has been recognized as an important strategy to modify the performance of materials, especially cathode materials for ZIBs [114]. Defect (including heteroatom doping, intrinsic defects, vacancy defects, *etc*.) can enhance ion diffusion and electron transfer by changing the atomic structure and charge distribution. Specifically, the introduction of defects into electrode materials can not only increase the storage site of foreign ions and effectively improve the capacity of batteries, but also generate a large number of active sites, which can effectively promote the kinetics of electrochemical reactions [115]. In particular, Oxygen vacancy, which can greatly enhance ion diffusion kinetics, has been considered as a major defect for tuning the electronic structure and physicochemical properties of cathode materials [3,114,116]. Therefore, designing an ammonium vanadate cathode with abundant oxygen defects is very important to obtain excellent Zn^{2+} storage capacity [117].

Oxygen-deficient $NH_4V_4O_{10-x}$ nH_2O (NVOH) microspheres assembled by nanoplates were synthesized by He et al. [118]. The experimental tests are conducted to demonstrate that the oxygen vacancies enable fast Zn^{2+} diffusion and good electrochemical performance. Furthermore, Bai and coworkers [119] first prepared an advanced stainless steel (SS) supported oxygen-rich vacancy $(NH_4)_2V_{10}O_{25}$ $8H_2O$ cistern-like nanobelt cathode with the mass of glucose 0.2 g (O_d-NVO-SS-2) (Fig. 6g and h). Through DFT calculations, it is known that the introduction of defects can reduce the adsorption energy of Zn^{2+} on the material surface (Fig. 6i), which is beneficial to increase the active sites of the electrode materials and provide additional capacity. As a result, the specific capacity of O_d-NVO-SS-2 reached 331.4 mAh g^{-1} at 0.3 A g^{-1} after 50 cycles, which is about 1.8 times that of NVO-SS (178.4 mAh g^{-1}).

Cation defect is also an effective defect method to help improve Zn^{2+} diffusion kinetics and increase electrochemical active sites for energy storage of the cathode materials. He et al. [35] designed $Zn_{0.3}(NH_4)_{0.3}V_4O_{10}$ $0.91H_2O$ (ZNV) microsphere cathode with abundant cation vacancies and pre-intercalated Zn^{2+} in the interlayers for AZBs. The ZNV cathode demonstrates outstanding electrochemical performances even at low temperature (more than 90 % capacity retention after 3500 cycles at 2 A g^{-1}) owing to the synergistic effect of the cation vacancies, the pre-intercalated Zn^{2+}, and the structural water molecules.

4.2.2.4. Doping engineering. Doping is to change the distribution state of holes and free electrons in the materials by introducing foreign atoms to occupy or replace the position of the lattice lattice point of the body, thereby enhancing the ionic conductivity and structural stability of the electrode materials. In other words, doping is also a kind of defect. Doping of metal elements such as Ti [120], Mn [121], Na [122] and Zr [123] has been certified to productively optimize the electrochemical properties of cathode materials, consequently leading to improve cycling stability, enhance electrical conductivity and facilitate ion diffusion.

In a recent study, He et al [16] synthesized Ti-doped $NH_4V_4O_{10}$ (NVO-Ti) nanobelts (Fig. 6j). From the TEM images of NVO-Ti and NVO electrodes in the discharged state after 2000 cycles, where the NVO electrode was severely damaged while NVO-Ti still maintained a good morphology (Fig. 6k), indicating that Ti-doping provides better structural stability.

In addition, since the crystal structure of molybdenum-based oxides is similar to that of vanadium-based oxides [124], Mo is chosen as the doping element for ammonium vanadate. Wang et al. [125] obtained a Mo-doped $NH_4V_4O_{10}$, whose interlayer spacing is expanded by the Mo insertion, which can provide more space for the intercalation of Zn^{2+}. Using the optimized Mo-doped $NH_4V_4O_{10}$ as cathode for ZIBs, it exhibited a high capacity of 335.0 mAh g^{-1} at 0.1 A g^{-1}.

4.2.2.5. Intercalation engineering. Intercalation is another effective modification strategy that introduces metal ions [35,126,127], molecular water [127–129] or polymers [130] as pillars between the [VO_n] layers of the layered ammonium vanadate to increase the interlayer spacing for rapid ion diffusion and stabilize the structure of the materials for ZIBs during Zn^{2+} de/intercalation process.

Using metal ions as "pillars" to intercalate the layered ammonium vanadate is a kind of sensible method to effectively improve electrochemical performance. Wang et al. [35] combined the strategies of pre-intercalation of Zn^{2+} and cation-deficient structure to prepare cation-deficient $Zn_{0.3}(NH_4)_{0.3}V_4O_{10}$ $0.91H_2O$ (ZNV) microsphere cathode, in which the partly pre-intercalated Zn^{2+} ions and structural water act as pillar to stabilize the structure of ZNV. Besides, Cao's group [21] reported that potassium ammonium vanadate (KNVO) was obtained by partially replacing ammonium ions in the interlayer of $NH_4V_4O_{10}$ (NVO) with K^+ incorporation (Fig. 6l). When these two materials were used as cathodes for ZIBs, KNVO was surprisingly found to have better electrochemical performance (discharge capacity of 464 mAh g^{-1} at 0.1 A g^{-1} and 90 % retention at 5 A/g after 3000 cycles, shown in Fig. 6m), which was mainly attributed to the increased oxygen vacancies due to the incorporation of K^+. On the other side, the incorporation of K^+ might prevent the irreversible deammoniation and thus enhance the stability of the whole structure. In another study, Chen et al. [126] fabricated $(NH_4)_2V_6O_{16}$ $1.5H_2O$ (NVO) nanostructures via a facile microwave-assisted hydrothermal reaction. The trapped $Zn(H_2O)_6^{2+}$ ions in the interlayer not only helped stabilize the vanadium oxide layer but also provided enough interlayer spacing for fast ion kinetics during the subsequent insertion/extraction. Thence the NVO cathode displayed a high specific capacity of 385 mAh g^{-1} at 0.1 A g^{-1}.

However, intercalated metal ions may have strong electrostatic interactions with anions in the host materials in aqueous electrolytes and the large molecular weight and volume of metal ions will cause an unstable change upon repeated Zn^{2+} de/intercalation [130,131]. Exactly, molecular water could act as an electrostatic shield and a "lubricant" to facilitate Zn^{2+} diffusion; NH_4^+ with the lower molecular weight could provide higher specific gravimetric and volumetric capacities, both of which can solve the above problems [132]. Particularly, Zhu et al. [106] reported an $NH_4V_4O_{10}$ $0.28H_2O$ (NHVO) microflower aqueous ZIB cathode material with NH_4^+ and structural water pre-intercalated in the vanadium oxide layers. The existence of NH_4^+ and structural water co-assisted the Zn^{2+} intercalation/de-intercalation, demonstrating superior discharge capacity of 410 mAh g^{-1} at 0.2 A g^{-1}.

Besides metal ions and structural water, polymers have also been used as promising pillars to design the cathode structure. For instance, Bin et al. [130] employed PEDOT intercalated $NH_4V_3O_8$ (PEDOT-NVO) as cathode materials, which made the interplanar spacing enlarged from 7.8 to 10.8 Å. As a result, this cathode showed a high capacity of 356.8 mAh g^{-1} at 0.05 A g^{-1} and superior cycling stability.

We all know that the ultimate goal of modification of electrode materials is to greatly improve the electrochemical performance. Therefore, if modifications are carried out, it should be considered whether the conductivity, structural stability, active sites, functionality, etc. of the materials have been improved. When doping, the selected dopant should be stable in the new structure and the radii of both should be as close as possible so that the dopant can enter the crystal lattice of the substrate smoothly. Moreover, the doped counterparts should be variable so as to adjust the amount of dopant to optimize the performance of the materials. Meanwhile, heterostructure is also a promising strategy [133]. In addition, the electrode can be optimized by adjusting the proportion of active materials in the electrode [134]. Of course, the electrolyte can also be optimized, but the study in this area needs to be further explored so that the better modification strategies can be found to enhance the electrochemical performance of ZIBs.

It is self-evident that defects, doping and other modifications have an effect on electrode materials, but their mechanism is still elusive. Advanced *in situ* characterization techniques, such as Fourier transform infrared, Raman, synchrotron radiation, etc., can be used to monitor the doping, defect formation or other transformation processes of the electrode materials, which is conducive to the research of the mechanism and provides theoretical guidance for further modification. In addition, these modification strategies also provide meaningful reference value for improving the performance of AMPs and AMMs and making them more suitable for energy storage.

4.2.3. Other batteries

Ammonium salts are not only widely used in LIBs and ZIBs, but also

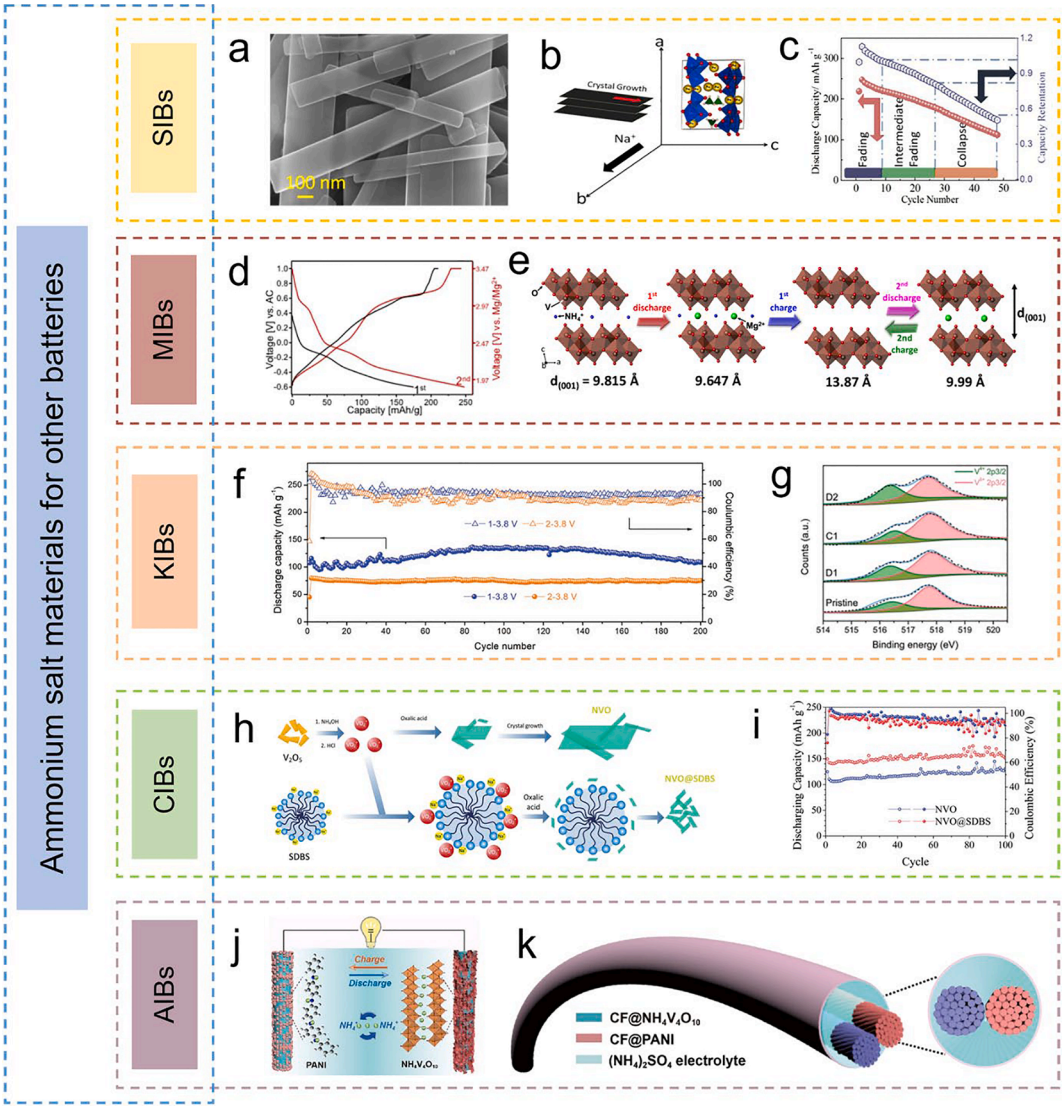

Fig. 7. Ammonium salt materials for other metal-ion batteries. (a) FEG-SEM image of $NH_4V_4O_{10}$. (b) Graphical representation of $NH_4V_4O_{10}$ nano-belts growth. (c) Discharge capacity and capacity retention vs cycle number of $NH_4V_4O_{10}$ cathode. (a-c) Reproduced with permission [142]. Copyright 2015, American Chemical Society. (d) Discharge-charge profiles for $NH_4V_4O_{10}$ at a 0.2 C rate for the first and second cycles. (e) An illustration of the evolution of $NH_4V_4O_{10}$ structure upon cycling. (d, e) Reproduced with permission [144]. Copyright 2018, American Chemical Society. (f) Cycling performance of NVO at 50 mA g^{-1} in 1/2–3.8 V. (g) V 2p core-level XPS spectra of NVO after the first discharge (D1), first charge (C1), and second discharge process (D2). (f, g) Reproduced with permission [136]. Copyright 2018, Wiley-VCH. (h) Schematic illustration of the preparation and (i) Comparison of the cycling performance of NVO and NVO@SDBS. (h, i) Reproduced with permission [137]. Copyright 2018, The Royal Society of Chemistry. Schematic illustration of (j) aqueous NH_4-ion full cell and (k) fiber-shaped NH_4-ions full cells. (j, k) Reproduced with permission [138]. Copyright 2019, Elsevier.

used in other metal-ion batteries such as SIBs [135], MIBs [30], KIBs [136], Ca-ion batteries [137] and NH_4-ion batteries [138], which are expected to be the alternatives of LIBs.

4.2.3.1. Na-ion batteries. Sodium-ion batteries (SIBs) have been developed as the promising and more sustainable candidate for LIBs, mainly because of the relatively abundant and lower cost sodium resources compared to lithium [139,140]. Especially, the physicochemical properties of sodium are similar to that of lithium [141], which leads some researchers to develop SIBs based on LIBs.

Sarkar and co-workers [142] synthesized 1D $NH_4V_4O_{10}$ nanobelts (Fig. 7a) as cathode material for Na^+ storage. From Fig. 7b, $NH_4V_4O_{10}$ nano-belts elongate toward the *c*-axis and minimally grow toward the *b*-axis (*i.e.*, [0 k 0]), which accelerates the transport of Na^+. Further improvement in electrochemical performances was demonstrated by the use of carbon coated Al-current collector between potential cut-off of 1.5–3.5 V. This material delivered initial discharge capacity ~225 mAh g^{-1} at high current rate of 0.2 A g^{-1} and good cyclic stability (Fig. 7c). However, its theoretical capacity for the intake of $3Na^+$ ions is ~210.5 mAh g^{-1}, of which the extra capacity may be attributed to reduction of V^{4+} to V^{3+} or interfacial surface storage of Na^+.

In addition, some efforts have also been made to explore anode materials for SIBs. Yao et al. [139] used *in situ* TEM method to investigate the sodium storage mechanism of layered $NH_4V_4O_{10}$ as anode material for SIBs, revealing a stepwise Na-storage reaction mechanism. However, pure ammonium vanadate often suffers from structural fragility and low capacity. To response these problems, K-doped $(NH_4)_2V_3O_8$/graphene were developed by Liu et al. [143]. Benefiting from the advantages that flexible graphene can stabilize the structure and K doping can expand the interlayer spacing of $(NH_4)_2V_3O_8$, the composite manifested excellent cycling stability and a good rate performance with a reversible capacity of 235.4 mAh g^{-1} at 0.1 A g^{-1} during the 100th cycle.

4.2.3.2. Mg-ion batteries. Because of the abundant resource of magnesium in the earth's crust and improved safety, Mg-ion batteries (MIBs) have also been regarded as the substitution of LIBs [123,144,145]. However, there is still the problem of slow diffusion of Mg^{2+} in the host structure, resulting in very limited materials for MIBs. Great efforts have been made by researchers to develop the host structures for magnesium ions. For example, $NH_4V_4O_{10}$, stabilized in a layered structure, was a suitable choice as a host for MIBs due to the ability to create large interlayer distances. Esparcia and co-workers [144] demonstrated reversible magnesiation in $NH_4V_4O_{10}$ using 0.5 M $Mg(ClO_4)_2$ in acetonitrile as the electrolyte with an initial discharge capacity of 174.8 mAh g^{-1} at 0.2 C rate and the average discharge voltage of about 2.31 V (vs Mg/Mg^{2+}) (Fig. 7d). As depicted in Fig. 7e, we can see that after the extraction of NH_4^+ ions, the subsequent cycles mainly involved the reversible Mg^{2+} intercalation/deintercalation.

4.2.3.3. K-ion batteries. K-ion batteries (KIBs) have also been regarded as a promising alternative energy system to LIBs because of the abundance of the K resource and similar electrochemical properties to LIBs. Besides, K has a lower standard redox potential than Li, which makes KIB system show a potentially higher cell voltage [146].

Xu et al. [136] studied the electrochemical properties of $NH_4V_4O_{10}$ (NVO) in KIBs. NVO delivered a high capacity of 136 mAh g^{-1} at 0.05 A g^{-1} and a decay rate of 0.02 % per cycle over 200 cycles in the range of 1–3.8 V (Fig. 7f), demonstrating the material's excellent rate capability. Electrochemical mechanism was also studied using *ex situ* XPS, which suggested that K-ion storage in NVO is a topotactic process, where transition between V^{4+} and V^{5+} occurs (Fig. 7g). Fan et al. [147] further investigated the effect of interlayer spacing and preintercalated cations of the vanadate nanowires on their KIB performance. Compared to $NH_4V_3O_8$ nanowires (d_{100} of 7.80 Å), $(NH_4)_{0.5}V_2O_5$ nanowires (d_{100} of 9.52 Å) showed a faster K^+ diffusion and much higher reversible capacity. Importantly, the preintercalation of K^+ into V–O slabs is also crucial to the stability of the structure, which leads to better electrochemical cycling stability in $K_{0.5}V_2O_5$ among these vanadate materials.

4.2.3.4. Ca-ion batteries. Similar to MIBs, there are only a few materials for Ca-ion batteries (CIBs) because of the difficulty in electroplating Ca metal in conventional electrolytes. To improve the properties of electrode materials, Ngoc Vo et al. [137] added the surfactant sodium dodecylbenzenesulfonate (SDBS) into $NH_4V_4O_{10}$ to synthesize NVO@SDBS as cathode material for CIBs (Fig. 7h). Thanks to the Na-doping effect, the surfactant-assisted process not only decreased the particle size but also increased the active site proportion of V^{4+}/V^{5+}, which makes the NVO@SDBS cathode show high coulombic efficiency and outstanding cyclic stability (Fig. 7i). As a result, this material could be a potential cathode material for practical applications in CIBs.

4.2.3.5. NH_4-ion batteries. Recently, Ammonium-ion batteries (AIBs) (Fig. 7j) have become an emerging technology in battery systems, in which NH_4-ions are used as effective charge carriers due to their abundancy, light weight (low molar mass of 18 g mol^{-1}) and fast diffusion kinetics (small hydration ion size of 3.31 Å), offering low cost and attractive performance [148,149].

In order to rapidly advance the practical application of AIBs, researchers are committed to searching layered NVO cathode materials that can accommodate massive NH_4^+ ions because of their large interlayer spacings. For example, Li et al. [138] assembled a full AIB with urchin-like $NH_4V_4O_{10}$ coated on CF as cathode and PANI nanorods grown on CFs as anode in $(NH_4)_2SO_4$ aqueous electrolyte (Fig. 7k). The aqueous AIB could exhibit a high specific capacity of 167 mAh g^{-1} at 0.1 A g^{-1}. Unfortunately, the use of liquid-state aqueous electrolyte may cause side reactions caused by water hydrolysis, thus affecting the lifespan and long-term stability of batteries [150]. To overcome this limitation, Kuchena and co-workers [150] fabricated a full flexible AIB consisting of a concentrated hydrogel electrolyte sandwiched between the $NH_4V_3O_8$ $9H_2O$ nanobelts cathode and the PANI anode. Electrochemical test results show that the battery based on the gel electrolyte shows the highest initial capacity of 55 mAh g^{-1} at 0.1 A g^{-1} and outstanding performance, which can be attributed to the reduced side reactions resulted from the high salt concentration.

Besides NVOs, two other candidates, AMPs and AMMs, are also presented in this paper for electrochemical energy storage. However, for AMPs, it is more used in SCs because of its rapid ion and electron transport and high theoretical capacitance to improve energy density of SCs, but rarely used in batteries, especially multivalent metal ion batteries; for AMMs, the application development of this ammonium salt is still in the initial stage, and there are very few reports about its use in electrochemical energy storage devices. To promote the development of AMPs and AMMs, it is necessary to design them reasonably to optimize their performance and make them suitable for energy storage. Like designing NVOs, we can modify the structures of AMPs and AMMs (including composites, defects, doping and intercalation) to improve their electrochemical performance. Particularly, constructing defects into electrode materials can provide more ion storage sites and active sites, promote ion diffusion and charge transfer, and maintain structural stability, which is a good choice for designing AMPs and AMMs.

5. Advanced characterization techniques

At present, advanced characterization techniques (like *in situ* XRD, *in situ* TEM, and *in situ* Raman spectra, *etc.*) can realize real-time observation of materials to obtain more comprehensive information, which have been more and more applied in material characterization [151].

5.1. *In situ* XRD

For *in situ* XRD technique, it is an effective test method that can realize real-time monitoring of phase transition and structural evolution of electrode materials. Bin et al. [152] used *in situ* XRD to investigate the structure information of $(NH_4)_{0.5}V_2O_5$ at complete charge state. The evolution of XRD patterns of the $(NH_4)_{0.5}V_2O_5$ showed a new set of peaks at 16.2 and 27.6°, which indicated that a new phase of $Zn_x(NH_4)_{0.5}V_2O_5$ is produced from the increased insertion of the Zn^{2+}. Similarly, the structural changes of CF@$NH_4V_4O_{10}$ under different electrochemical states were also investigated in detail by Li et al. [138] using *in situ* XRD. The (0 0 1) peak of CF@$NH_4V_4O_{10}$ positively shifted to 9.21° with the interlayer spacing decreasing to 9.59 Å when charged to 1.0 V, corresponding to the de-intercalation of NH_4^+; while the discharge process was opposite, the (0 0 1) peak shifted to the low angle, and the lattice parameter obviously increased due to the insertion of NH_4^+ and the formation of N—H···O bonds. To get an insight into the formation of new phase of $(NH_4)_2V_6O_{16}$ 1.5H_2O upon Mg^{2+} insertion, *in situ* XRD characterization (Fig. 8a) was performed in a narrow 2θ range only focusing on the (0 0 2) reflection [145]. Results showed that the (0 0 2) reflection moved to a higher angle during discharge, revealing the existence of an intermediate phase $Mg^{2+}_{1.22}(NH_4)_2V_6O_{16}$ 1.5H_2O due to the insertion of Mg^{2+} ions. Additionally, in the study of Hong et al. [86], who used *in situ* XRD analysis to elucidate the structural change of $(NH_4)_2V_7O_{16}$ during cycling. The complex changes in structure can be seen from the (0 0 l) peak and the appearance/disappearance of new peaks in the first cycle.

5.2. *In situ Raman spectra*

In addition, *in situ* Raman spectra which usually was used to further explore the electrochemical reaction mechanism of electrode materials was also used. Both of Zhu et al. [106] and Cao et al. [3] used *in situ* Raman spectra to probe the reversibility of Zn^{2+} extraction/insertion of ammonium vanadate materials during charge/discharge. In Zhu's study, *in situ* Raman spectra showed that four new bands appeared at 100, 185, 300, and 775 cm^{-1} and Fig. 8b of Cao's study appeared five peaks at approximately 200–1200 cm^{-1} caused by V–O–V bending and V–O stretching vibrations during the charge state. These new bands and peaks mentioned above gradually disappeared during the subsequent discharge process and finally recovered to the original state, revealing the good reversibility of the electrochemical process. Simultaneously, the above process also demonstrated the charge transfer process of the V^{5+}/V^{4+} redox pair.

5.3. *In situ TEM*

Besides *in situ* XRD and *in situ* Raman spectra, *in situ* TEM was also used to characterize morphological evolution and phase transformation of materials. For example, Yao et al. [139] applied *in situ* TEM and *in situ* ED patterns to study the state of the phase in real-time during the sodiation/desodiation of $NH_4V_4O_{10}$ anode, revealing a stepwise Na-storage reaction mechanism. During the first sodiation process, there is a two-step phase transformation mechanism involving the initial intercalation reaction that results in $Na_xNH_4V_4O_{10}$ phase and the following conversion reaction with the final formation of V_2O_3 phase ((1 0 4), (1 1 0), (1 1 6), and (3 0 0) planes) and Na_2O phase ((2 2 0) and (4 2 0) planes) (Fig. 8c). While during the subsequent desodiation process, the V_2O_3 phase can only be oxidized to VO_2 phase ((1 3 0), (1 5 1), and (2 5 0) planes) (Fig. 8d) rather than the original NVO phase, demonstrating the asymmetric conversion reaction for the first discharge-charge cycle. After that, from the repeated (de)sodiation cycles and ED analysis we can know that a reversible phase transformation between V_2O_3 and VO_2 is responsible for the long-term Na-storage cycling stability.

The experimental results of advanced *in situ* characterization technology are very sensitive to structural characteristics. In addition, other technologies (such as *in situ* XPS, XAS, AFM) are also worth exploring in the future research. In near future, the micro-morphology of electrode materials can be accurately constructed by programming, 3D printing and so on. All these technologies will provide a deeper insight into the mechanism of energy storage.

6. Theoretical calculation methodology

First-principles calculations based on DFT are to recognize the physical and other properties of materials at the atomic level, a very effective tool for calculating the microstructure and properties of crystalline materials. By using first-principles calculations, it is possible to deeply understand the changes of the structure and electrochemical

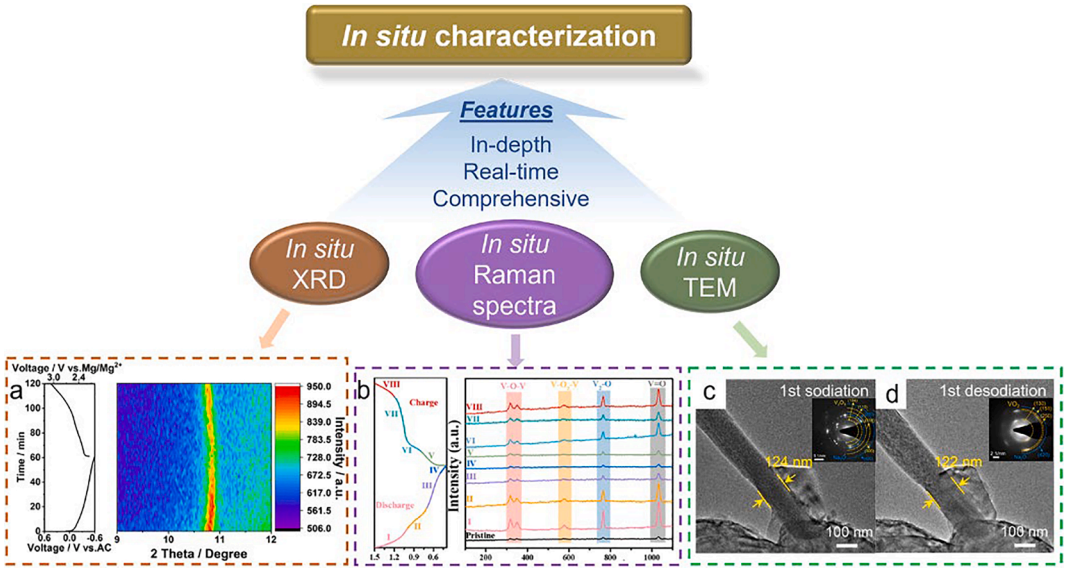

Fig. 8. *In situ* characterization techniques of ammonium salt materials. (a) *In situ* XRD patterns of NHVO-H_2O during the first cycle. (a) Reproduced with permission [145]. Copyright 2021, American Chemical Society. (b) *In-situ* Raman spectroscopy of oxygen defect enriched $(NH_4)_2V_{10}O_{25}$ 8H_2O cathode. (b) Reproduced with permission [3]. Copyright 2021, Elsevier. *In-situ* TEM observation of the morphological evolution of NVO NB electrode during the first (c) sodiation and (d) desodiation cycle; the insets are corresponding ED patterns of the (de)sodiated NVO NB. (c, d) Reproduced with permission [139]. Copyright 2021, Elsevier.

properties of ammonium salt materials during electrochemical processes [105,153]. Based on first-principles calculations, Sarkar and co-workers [153] investigated the structural transformation of the δ-$NH_4V_4O_{10}$ electrode during Li/Na insertion. Fig. 9a and b illustrated the changes in the VO_n polyhedral coordination, as a function of the concentration × of Li^+/Na^+ in δ-$NH_4V_4O_{10}$. When Li^+ concentration up to $x > 2$ in $Li_xNH_4V_4O_{10}$, the coordination polyhedra of V5 and V8 changed from DO to TrB. On the contrary, the V6–V7 coordination polyhedra changed from TrB to DO at $x = 1$ during insertion of Na^+ into δ-$NH_4V_4O_{10}$, suggesting two distinct mechanisms of structural distortion in δ-$NH_4V_4O_{10}$. Moreover, we can see from Fig. 9c and d that the energy barrier of Zn^{2+} diffusion along [0 1 0] direction (0.63 eV) was lower than that through a VO layer (2.89 eV) in monoclinic $NH_4V_4O_{10}$ by first-principles calculations, revealing the feasibility of monoclinic NVO to provide fast Zn^{2+} ion intercalation along the [0 1 0] direction in the interlayer space [105].

In order to deeply explore the effect of structural engineering on ammonium salt materials during the discharging-charging process, Xiang et al. [119] investigated the role of oxygen vacancies by calculating the total density states (TDOS) and projected density of states (PDOS) (Fig. 9e and f). The results showed that defect engineering of NVO can reduce the band gaps, thereby improving the electronic conductivity and Zn^{2+} diffusion coefficient. Also in another study, it was confirmed by DFT calculations (Fig. 9g and h) that KNVO with abundant oxygen vacancies after incorporation of K^+ into NVO had a better diffusion path and a lower diffusion barrier, thereby accelerating the kinetics of Zn^{2+} ion intercalation [21]. Furthermore, first-principles calculations were conducted to get insight into the Mg^{2+} storage properties of $(NH_4)_2V_6O_{16}$ 1.5H_2O (NHVO-H_2O) [145]. As shown in Fig. 9i, the calculated value of maximum electrostatic potential for NHVO-H_2O (−16.20 eV) was smaller than that for NHVO (−16.95 eV). It was also confirmed by CI-NEB calculations that determined the diffusion kinetics of Mg^{2+} in NHVO-H_2O and NHVO (Fig. 9j). All the results indicated that Mg^{2+} can migrate more easily in the NHVO-H_2O electrode without atom directly blocking Mg^{2+} (Fig. 9k and l).

In summary, both advanced characterization technologies and theoretical calculation methods can certainly deepen provide deep insights into material structure, properties and energy storage mechanism.

7. Conclusions and perspectives

In general, this review mainly focused on describing the applications with respect to several common ammonium salt materials for SCs and batteries. Emerging as a new class of layered materials, ammonium salt materials have attracted tremendous research interest and are considered as one of the most promising electrode materials for advanced energy storage devices due to their abundant resources, simple synthesis, low cost, and high specific capacity. Thanks to the introduction of NH_4^+ ions and the unique layered structure, ammonium salt materials exhibit high theoretical charge storage capacity and abundant electroactive sites, thus achieving excellent electrochemical performance. However, it should be noted that although ammonium salt materials have made much progress in the field of energy storage, there are still some problems to be solved, such as low electrical conductivity and poor cycle stability, which are the primary obstacles of ammonium salt materials and limit their large-scale applications. In the face of these problems and in order to promote the more mature development and application of this new electrode material, future research should also focus on the following directions (Fig. 10):

(i) As for synthetic methods, the most common preparation methods for ammonium salt materials are still the hydrothermal-based

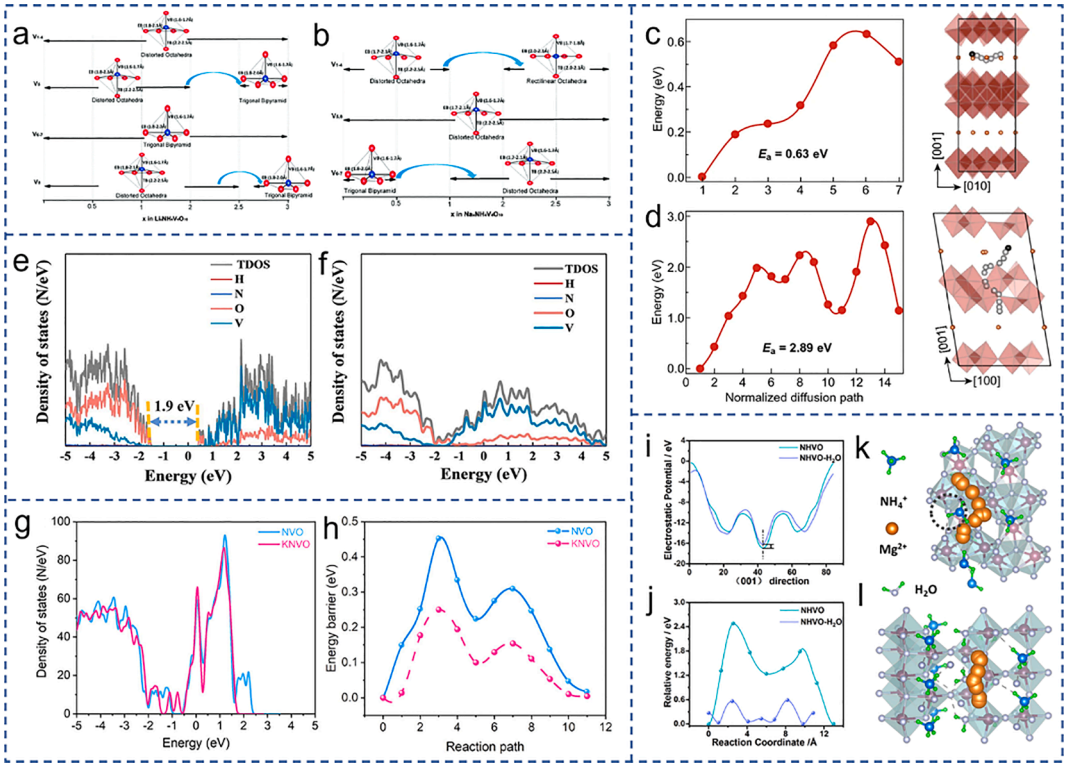

Fig. 9. Change in vanadium coordination polyhedra with concentration (x) of (a) Li^+ and (b) Na^+ in the host structure δ-$NH_4V_4O_{10}$. (a, b) Reproduced with permission [153]. Copyright 2016, The Royal Society of Chemistry. Calculated minimum energy paths of Zn^{2+} ion diffusion along (c) [0 1 0] and (d) [0 0 1] in monoclinic $NH_4V_4O_{10}$. (c, d) Reproduced with permission [105]. Copyright 2020, Springer Nature. TDOS and PDOS of (e) NVO-SS and (f) O_d-NVO-SS-2. (e, f) Reproduced with permission [119]. Copyright 2021, Elsevier. (g) Density of states and (h) Calculated Zn^{2+} diffusion barriers for paths of NVO and KNVO. (g, h) Reproduced with permission [21]. Copyright 2022, American Chemical Society. (i) Electrostatic potential, (j) calculated diffusion barrier, and diffusion pathway for Mg^{2+} in (k) NHVO and (l) NHVO-H_2O electrodes. (i–l) Reproduced with permission [145]. Copyright 2021, American Chemical Society.

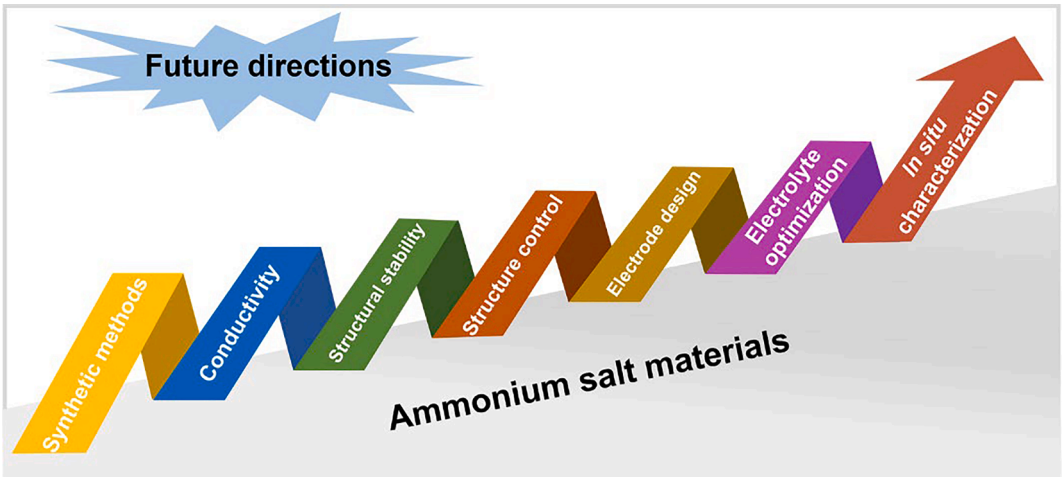

Fig. 10. A summary of future directions to be considered for the application of ammonium salt materials in energy storage devices.

routes. Although these methods can synthesize improved performance materials to a certain extent, they are limited to the experimental level due to their complex synthesis process and conditions, which restricts large-scale synthesis and is difficult to achieve commercial application. Therefore, extensive experiments are needed to explore more simple, feasible and efficient synthetic methods (such as sol–gel method) to achieve large-scale production, which will be particularly important in future development.

(ii) From the previous research results, low electrical conductivity is one of the main obstacles encountered in the application of ammonium salt materials in the field of energy storage. In response to this problem, researchers have proposed various methods to address it. Compositing ammonium salt materials with carbon matrix materials (such as graphene and CNTs) is the most suitable tool to overcome this disadvantage. Nevertheless, the introduction of graphene and CNTs not only increases the cost and dead mass, but also reduces the tap density which results in low energy density. As a result, more economical and practical strategies to improve electrical conductivity need to be explored.

(iii) In terms of structural stability, most ammonium salt materials suffer from low cycle stability, which is another major bottleneck restricting the further development of ammonium salt materials. Effectively controlling the structural changes of materials during charging and discharging plays a key role in improving the cycling performance. Surface-coated carbon materials and electrolyte engineering can suppress electrode dissolution. In addition, strategies such as constructing core@shell nanostructure, metal doping and defect engineering can also significantly increase the rate capability and cycle life.

(iv) Precise structural control has been shown to greatly improve the electrochemical performance of the materials. People have synthesized ammonium salt materials with different morphologies and sizes by adjusting the type and ratio of solvents. Porous structural materials have high specific surface area, which can provide more active centers, thereby accelerating ion/electron transport. 3D nanostructured materials can avoid the disadvantages of poor cycling and rate performance caused by severe self-aggregation of low-dimensional nanomaterials, while retaining their good specific capacity. Additionally, hierarchical materials possess complex assembly structures and unique ionic/electrical propagation capabilities, which can enhance SC performance at large load current densities.

(v) Reasonable electrode design can effectively promote ion/electron transfer, and ensure uniform dispersion of active particles, thereby achieving optimal performance of devices. During the manufacturing process of the electrode, it is inevitable to add binders and conductive agents. Traditional binder PVDF severely hinders metal ion transmission at the interface of the current collector/active materials. Other binders like carboxymethyl cellulose (CMC) and alginate exhibit better performance compared to PVDF. At the same time, it is encouraged to develop eco-friendly binders such as polyvinyl acetate (PVAc), polydopamine (PDA), natural cellulose, and so on for electrode preparation.

(vi) In addition to electrodes, electrolytes also play a role in the electrochemical behavior. Traditional aqueous electrolytes may suffer from side reactions and depletion of water content, affecting the lifetime and long-term stability of energy storage devices. Therefore, it is important to optimize electrolytes (optimize the salt concentration, select the optimum pH, *etc.*). In addition, hydrogel electrolytes (*e.g.*, PVA, PAM, etc) exhibit better electrochemical performance than aqueous electrolytes for some ammonium salt materials. However, many aspects regarding the nature of interphases created by hydrogel electrolytes remain elusive and require further investigation through characterization techniques.

(vii) *In situ* characterization techniques and advanced simulation techniques for studying the structural changes and energy storage mechanisms of ammonium salt materials during electrochemical processes are rarely mentioned in the literature, especially for AMPs and AMMs. For a deeper understanding of structure–property correlations, more comprehensive advanced characterization methods should be used.

In short, ammonium salt materials still challenging for use in EES devices, such as the lack of researches on ammonium metal molybdate and other potential ammonium salts, the elusive reaction and modification mechanism, and so on. There is no doubt that the achievements of ammonium salt materials in the field of energy storage are encouraging. We firmly believe that the above challenges will be gradually overcome by combining theories with experiments in the future research and the ammonium salt materials will exert greater application potential.

Declaration of Competing Interest

The authors declare that they have no known competing financial interests or personal relationships that could have appeared to influence the work reported in this paper.

Data availability

No data was used for the research described in the article.

Acknowledgements

The authors gratefully acknowledge financial support from the National Natural Science Foundation of China (No. 21676036), the Graduate Research and Innovation Foundation of Chongqing (No. CYB22043 and CYS22073), and the Large-scale Equipment Sharing Fund of Chongqing University (No. 202103150115).

References

[1] S. Chu, Y. Cui, N. Liu, The path towards sustainable energy, Nat. Mater. 16 (2017) 16–22, https://doi.org/10.1038/nmat4834.
[2] B. Dunn, H. Kamath, J. Tarascon, Electrical Energy Storage for the Grid: A Battery of Choices, Science 334 (2011) 928–935, https://doi.org/10.1126/science.1212741.
[3] J. Cao, D. Zhang, Y. Yue, X. Wang, T. Pakornchote, T. Bovornratanaraks, X. Zhang, Z. Wu, J. Qin, Oxygen defect enriched $(NH_4)_2V_{10}O_{25}{\cdot}8H_2O$ nanosheets for superior aqueous zinc-ion batteries, Nano Energy 84 (2021), 105876, https://doi.org/10.1016/j.nanoen.2021.105876.
[4] K. Raju, H. Han, D. Velusamy, Q. Jiang, H. Yang, F. Nkosi, N. Palaniyandy, K. Makgopa, Z. Bo, K. Ozoemena, Rational Design of 2D Manganese Phosphate Hydrate Nanosheets as Pseudocapacitive Electrodes, ACS Energy Lett. 5 (2020) 23–30, https://doi.org/10.1021/acsenergylett.9b02299.
[5] Q. Cheng, X. Zhao, G. Yang, L. Mao, F. Liao, L. Chen, P. He, D. Pan, S. Chen, Recent advances of metal phosphates-based electrodes for high-performance metal ion batteries, Energy Storage Mater. 41 (2021) 842–882, https://doi.org/10.1016/j.ensm.2021.07.017.
[6] H. Wang, Q. He, S. Liang, Y. Li, X. Zhao, L. Mao, F. Zhan, L. Chen, Advances and perspectives of ZIFs-based materials for electrochemical energy storage: Design of synthesis and crystal structure, evolution of mechanisms and electrochemical performance, Energy Storage Mater. 43 (2021) 531–578, https://doi.org/10.1016/j.ensm.2021.09.023.
[7] K. Raju, Ammonium metal phosphates: Emerging materials for energy storage, Curr. Opin. Electrochem. 21 (2020) 351–357, https://doi.org/10.1016/j.coelec.2020.03.019.
[8] W. Chen, M. Fan, M. Yue, S. Wang, J. Liu, Rational design of nano-structured ammonium manganese phosphate hydrate as lithium ion battery anode, Mater. Lett. 285 (2021), 129084, https://doi.org/10.1016/j.matlet.2020.129084.
[9] F. Zhan, H. Wang, Q. He, W. Xu, J. Chen, X. Ren, H. Wang, S. Liu, M. Han, Y. Yamauchi, L. Chen, Metal–organic frameworks and their derivatives for metal-ion (Li, Na, K and Zn) hybrid capacitors, Chem. Sci. 13 (2022) 11981–12015, https://doi.org/10.1039/D2SC04012C.
[10] L. Kou, L. Cao, J. Huang, J. Yang, Facile synthesis of reduced graphene oxide/$NH_4V_3O_8$ with high capacity as a cathode material for lithium ion batteries, Micro, Nano Lett. 12 (2017) 940–943, https://doi.org/10.1049/mnl.2017.0107.
[11] B. Huang, W. Wang, T. Pu, J. Li, C. Zhao, L. Xie, L. Chen, Rational design and facile synthesis of two-dimensional hierarchical porous $M_3V_2O_8$ (M = Co, Ni and Co-Ni) thin sheets assembled by ultrathin nanosheets as positive electrode materials for high-performance hybrid supercapacitors, Chem. Eng. J. 375 (2019), 121969, https://doi.org/10.1016/j.cej.2019.121969.
[12] D. Kundu, B. Adams, V. Duffort, S. Vajargah, L. Nazar, A high-capacity and long-life aqueous rechargeable zinc battery using a metal oxide intercalation cathode, Nat. Energy 1 (2016) 16119, https://doi.org/10.1038/nenergy.2016.119.
[13] P. He, G. Zhang, X. Liao, M. Yan, X. Xu, Q. An, J. Liu, L. Mai, Sodium Ion Stabilized Vanadium Oxide Nanowire Cathode for High-Performance Zinc-Ion Batteries, Adv. Energy Mater. 8 (2018) 1702463, https://doi.org/10.1002/aenm.201702463.
[14] B. Tang, G. Fang, J. Zhou, L. Wang, Y. Lei, C. Wang, T. Lin, Y. Tang, S. Liang, Potassium vanadates with stable structure and fast ion diffusion channel as cathode for rechargeable aqueous zinc-ion batteries, Nano Energy 51 (2018) 579–587, https://doi.org/10.1016/j.nanoen.2018.07.014.
[15] B. Tang, J. Zhou, G. Fang, F. Liu, C. Zhu, C. Wang, A. Pan, S. Liang, Engineering the interplanar spacing of ammonium vanadates as a high-performance aqueous zinc-ion battery cathode, J. Mater. Chem. A 7 (2019) 940–945, https://doi.org/10.1039/C8TA09338E.
[16] D. He, Y. Peng, Y. Ding, X. Xu, Y. Huang, Z. Li, X. Zhang, L. Hu, Suppressing the skeleton decomposition in Ti-doped $NH_4V_4O_{10}$ for durable aqueous zinc ion battery, J. Power Sources 484 (2021), 229284, https://doi.org/10.1016/j.jpowsour.2020.229284.
[17] N.u. Rehman Lashari, M. Zhao, Q. Zheng, X. He, I. Ahmed, Z. Su, S. Tangsee, X. Song, Enhanced Rate Capability and Cycling Stability of Novel Ammonium Vanadate Materials Used in Aqueous Li-Ion Batteries, Energy Fuels 35 (5) (2021) 4570–4576.
[18] Y. Liu, M. Xu, B. Shen, Z. Xia, Y. Li, Y. Wu, Q. Li, Facile synthesis of mesoporous $NH_4V_4O_{10}$ nanoflowers with high performance as cathode material for lithium battery, J. Mater. Sci. 53 (2018) 2045–2053, https://doi.org/10.1007/s10853-017-1619-z.
[19] H. He, Z. Shang, X. Huang, S. Tan, D. Sun, G. Xu, Y. Tang, H. Wang, Ultrathin $(NH_4)_{0.5}V_2O_5$ Nanosheets as a Stable Anode for Aqueous Lithium Ion Battery, J. Electrochem. Soc. 163 (2016) A2349-A2355. doi: 10.1149/2.1101610jes.
[20] C. Li, S. Wang, G. Wang, S. Wang, X. Che, D. Li, J. Qiu, $NH_4V_4O_{10}$/rGO Composite as a high-performance electrode material for hybrid capacitive deionization, Environ. Sci. Water Res. Technol. 6 (2020) 303–311, https://doi.org/10.1039/C9EW00499H.
[21] Q. Zong, Q. Wang, C. Liu, D. Tao, J. Wang, J. Zhang, H. Du, J. Chen, Q. Zhang, G. Cao, Potassium Ammonium Vanadate with Rich Oxygen Vacancies for Fast and Highly Stable Zn-Ion Storage, ACS Nano 16 (2022) 4588–4598, https://doi.org/10.1021/acsnano.1c11169.
[22] X. Wang, B. Xi, Z. Feng, W. Chen, H. Li, Y. Jia, J. Feng, Y. Qian, S. Xiong, Layered $(NH_4)_2V_6O_{16}{\cdot}1.5H_2O$ nanobelts as a high-performance cathode for aqueous zinc-ion batteries, J. Mater. Chem. A 7 (2019) 19130–19139, https://doi.org/10.1039/C9TA05922A.
[23] S. Carling, P. Day, D. Vissen, Crystal and Magnetic Structures of Layer Transition Metal Phosphate Hydrates, Inorg. Chem. 34 (1995) 3917–3927, https://doi.org/10.1021/ic00119a013.
[24] Y. Xie, X. Xiong, K. Han, Flake $(NH_4)_6Mo_7O_{24}$/Polydopamine as a High Performance Anode for Lithium Ion Batteries, Materials 14 (5) (2021) 1115.
[25] T. Ke, B. Vedhanarayanan, L. Shao, T. Lin, Porous and Hierarchically Structured Ammonium Nickel Molybdate/Nickel Sulfide/Reduced Graphene Oxide Ternary Composite as High Performance Electrode for Supercapacitors, ChemElectroChem 6 (2019) 3806–3814, https://doi.org/10.1002/celc.201900885.
[26] D. Levin, S. Soled, J. Ying, Chimie Douce Synthesis of a Layered Ammonium Zinc Molybdate, Chem. Mater. 8 (1996) 836–843, https://doi.org/10.1021/cm950427i.
[27] S. Wang, H. Pang, S. Zhao, W. Shao, N. Zhang, J. Zhang, J. Chen, S. Li, $NH_4CoPO_4{\cdot}H_2O$ microbundles consisting of one-dimensional layered microrods for high performance supercapacitors, RSC Adv. 4 (2014) 340–347, https://doi.org/10.1039/C3RA45977B.
[28] F. Liao, X. Zhao, G. Yang, Q. Cheng, L. Mao, L. Chen, Recent advances on two-dimensional NiFe-LDHs and their composites for electrochemical energy conversion and storage, J. Alloys Compd. 872 (2021), 159649, https://doi.org/10.1016/j.jallcom.2021.159649.
[29] Q. Li, Y. Li, H. Peng, X. Cui, M. Zhou, K. Feng, P. Xiao, Layered $NH_4Co_xNi_{1-x}PO_4{\cdot}H_2O$ ($0 \leqq x \leqq 1$) nanostructures finely tuned by Co/Ni molar ratios for asymmetric supercapacitor electrodes, J. Mater. Sci. 51 (2016) 9946–9957, https://doi.org/10.1007/s10853-016-0151-x.
[30] Q. Chen, Q. Xia, Y. Xu, P. Wang, Q. Tan, $NH_4V_4O_{10}$ micro-flowers as cathode material for high performance hybrid magnesium-lithium-ion batteries, Mater. Lett. 247 (2019) 178–181, https://doi.org/10.1016/j.matlet.2019.03.056.
[31] D. Fang, Y. Cao, R. Liu, W. Xu, S. Liu, Z. Luo, C. Liang, X. Liu, C. Xiong, Novel hierarchical three-dimensional ammonium vanadate nanowires electrodes for lithium ion battery, Appl. Surf. Sci. 360 (2016) 658–665, https://doi.org/10.1016/j.apsusc.2015.11.038.
[32] C. Wang, H. Liu, M. Jiang, Y. Wang, R. Liu, Z. Luo, X. Liu, W. Xu, C. Xiong, D. Fang, Ammonium vanadate@polypyrrole@manganese dioxide nanowire arrays with enhanced reversible lithium storage, Appl. Surf. Sci. 416 (2017) 402–410, https://doi.org/10.1016/j.apsusc.2017.04.069.
[33] H. Fei, X. Wu, H. Li, M. Wei, Novel sodium intercalated $(NH_4)_2V_6O_{16}$ platelets: High performance cathode materials for lithium-ion battery, J. Colloid Interface Sci. 415 (2014) 85–88, https://doi.org/10.1016/j.jcis.2013.10.025.
[34] X. Wang, Y. Wang, Y. Jiang, X. Li, Y. Liu, H. Xiao, Y. Ma, Y. Huang, G. Yuan, Tailoring Ultrahigh Energy Density and Stable Dendrite-Free Flexible Anode with $Ti_3C_2T_x$ MXene Nanosheets and Hydrated Ammonium Vanadate Nanobelts for Aqueous Rocking-Chair Zinc Ion Batteries, Adv. Funct. Mater. 31 (2021) 2103210, https://doi.org/10.1002/adfm.202103210.
[35] T. He, S. Weng, Y. Ye, J. Cheng, X. Wang, X. Wang, B. Wang, Cation- deficient $Zn_{0.3}(NH_4)_{0.3}V_4O_{10}{\cdot}0.91H_2O$ for rechargeable aqueous zinc battery with superior low- temperature performance, Energy Stor. Mater. 38 (2021) 389–396, https://doi.org/10.1016/j.ensm.2021.03.025.
[36] F. Theobald, J. Theobald, J. Vedrine, R. Clad, J. Renard, Crystal growth, structure, electron paramagnetic resonance and magnetic properties of $(NH_4)_2V_3O_8$, J. Phys. Chem. Solids 45 (1984) 581–587, https://doi.org/10.1016/0022-3697(84)90050-7.
[37] A. Ottmann, G. Zakharova, B. Ehrstein, R. Klingeler, Electrochemical performance of single crystal belt-like $NH_4V_3O_8$ as cathode material for lithium-ion batteries, Electrochim. Acta 174 (2015) 682–687, https://doi.org/10.1016/j.electacta.2015.06.027.
[38] Y. Zhang, J. Zheng, Q. Wang, S. Zhang, T. Hu, C. Meng, One-step hydrothermal preparation of $(NH_4)_2V_3O_8$/carbon composites and conversion to porous V_2O_5 nanoparticles as supercapacitor electrode with excellent pseudocapacitive capability, Appl. Surf. Sci. 423 (2017) 728–742, https://doi.org/10.1016/j.apsusc.2017.06.249.
[39] V. Koleva, T. Boyadzhieva, R. Stoyanova, Crystal and Morphology Design of Dittmarite-Type Ammonium Iron-Manganese Phosphates, $NH_4Mn_{1-x}Fe_xPO_4{\cdot}H_2O$, as Precursors for Phospho-olivine Electrodes, Cryst. Growth Des. 19 (2019) 3744–3754, https://doi.org/10.1021/acs.cgd.9b00094.
[40] G. Kiriukhina, O. Yakubovich, O. Dimitrova, Crystal structure of a new polymorphic modification of niahite, $NH_4MnPO_4{\cdot}H_2O$, Crystallogr. Rep. 60 (2015) 198–203, https://doi.org/10.1134/S106377451502011X.
[41] B. Liang, Y. Chen, J. He, C. Chen, W. Liu, Y. He, X. Liu, N. Zhang, V. Roy, Controllable Fabrication and Tuned Electrochemical Performance of Potassium

Co–Ni Phosphate Microplates as Electrodes in Supercapacitors, ACS Appl. Mater. Interfaces 10 (2018) 3506–3514, https://doi.org/10.1021/acsami.7b14552.
[42] D. Levin, S. Soled, J. Ying, Crystal Structure of an Ammonium Nickel Molybdate Prepared by Chemical Precipitation, Inorg. Chem. 35 (1996) 4191–4197, https://doi.org/10.1021/ic951200s.
[43] Z. Wang, J. Zhang, H. Wang, X. Wei, J. Zhang, H. Chen, S. Liu, S. Wei, X. Lu, Hydrothermal synthesis of ammonium vanadate $[(NH_4)_2V_7O_{16}{\cdot}3.6H_2O]$ as a promising zinc-ion cathode: Experimental and theoretical study of its storage, Electrochim. Acta 404 (2022) 139785.
[44] T. Raja, P. Vickraman, A. Justin, B. Reddy, Electrochemical studies on $NH_4MnPO_4{\cdot}H_2O$–rGO Hybrid Composite Synthesized via Microwave Route for High Energy Supercapacitors, J. Mater. Sci. 55 (2020) 14447–14463, https://doi.org/10.1007/s10853-020-05032-4.
[45] X. Guo, N. Li, Y. Cheng, G. Wang, Y. Zhang, H. Pang, General synthesis of nitrogen-doped metal (M = Co^{2+}, Mn^{2+}, Ni^{2+}, or Cu^{2+}) phosphates, Chem. Eng. J. 411 (2021), 128544, https://doi.org/10.1016/j.cej.2021.128544.
[46] C. Liu, H. Peng, L. Cao, X. Duan, Y. Zhang, P. Xiao, Liquid-phase exfoliation of $NH_4Co_{0.4}Ni_{0.6}PO_4{\cdot}H_2O$ for energy storage device, J. Alloys Compd., 701 (2017) 67-74. doi: 10.1016/j.jallcom.2017.01.123.
[47] G. Zakharova, A. Ottmann, B. Ehrstein, A. Tyutyunnik, Q. Zhu, S. Lu, V. Voronin, A. Enyashin, R. Klingeler, A new polymorph of $NH_4V_3O_7$: Synthesis, structure, magnetic and electrochemical properties, Solid State Sci. 61 (2016) 225–231, https://doi.org/10.1016/j.solidstatesciences.2016.10.003.
[48] M. Wang, Y. Zhao, X. Zhang, R. Qi, S. Shi, Z. Li, Q. Wang, Y. Zhao, Interface-rich core-shell ammonium nickel cobalt phosphate for high-performance aqueous hybrid energy storage device without a depressed power density, Electrochim. Acta 272 (2018) 184–191, https://doi.org/10.1016/j.electacta.2018.04.005.
[49] S. Ma, D. Xiang, Y. Wang, X. Hao, H. Li, Z. Liu, T. Zhang, J. Yang, G. Zhang, Ammonium nickel-cobalt phosphate nanoflowers on highly conductive carbon fibers as an electrode material for enhanced electrochemical performance supercapacitors, Asia-Pac. J. Chem. Eng. 17 (2022) e2749.
[50] C. Yin, L. Zhao, Z. Bai, H. Liu, Y. Liu, C. Liu, A novel porous ammonium nickel molybdate as the catalyst precursor towards deep hydrodesulfurization of gas oil, Fuel 107 (2013) 873–878, https://doi.org/10.1016/j.fuel.2013.02.001.
[51] B. Jia, M. Qin, Z. Zhang, S. Li, X. Wang, M. Huang, H. Wu, Z. Chen, X. Lu, L. Zhang, X. Qu, Square-nanosheet flowers with an ammonium vanadate phase and their transformation to VO_2(B) net-like nanosheets, J. Alloys Compd. 704 (2017) 79–88, https://doi.org/10.1016/j.jallcom.2017.02.046.
[52] H. Wang, K. Huang, S. Liu, C. Huang, W. Wang, Y. Ren, Electrochemical property of $NH_4V_3O_8{\cdot}0.2H_2O$ flakes prepared by surfactant assisted hydrothermal method, J. Power Sources 196 (2011) 788–792, https://doi.org/10.1016/j.jpowsour.2010.07.022.
[53] L. Kou, L. Cao, J. Huang, J. Song, L. Feng, Y. Wang, S. Chen, K. Kajiyoshi, Polyethylene glycol (PEG)-assisted synthesis of self-assembled cactus-like $NH_4V_3O_8$ for lithium ion battery cathode, Scr. Mater. 183 (2020) 75–80, https://doi.org/10.1016/j.scriptamat.2020.03.025.
[54] K. Raju, K. Ozoemena, Hierarchical One-Dimensional Ammonium Nickel Phosphate Microrods for High-Performance Pseudocapacitors, Sci. Rep. 5 (2015) 17629, https://doi.org/10.1038/srep17629.
[55] Y. Jiang, Z. Wu, F. Ye, R. Pang, L. Zhang, Q. Liu, X. Chang, S. Sun, Z. Sun, L. Hu, Spontaneous knitting behavior of 6.7-nm thin $(NH_4)_{0.38}V_2O_5$ nano- ribbons for binder-free zinc-ion batteries, Energy Stor. Mater. 42 (2021) 286–294, https://doi.org/10.1016/j.ensm.2021.07.045.
[56] S. Kim, V. Soundharrajan, S. Kim, B. Sambandam, V. Mathew, J. Hwang, J. Kim, Microwave-Assisted Rapid Synthesis of $NH_4V_4O_{10}$ Layered Oxide: A High Energy Cathode for Aqueous Rechargeable Zinc Ion Batteries, Nanomaterials 11 (8) (2021), https://doi.org/10.3390/nano11081905.
[57] G. Zakharova, A. Ottmann, B. Ehrstein, R. Klingeler, Microwave-assisted hydrothermal synthesis of $NH_4V_3O_8$ microcrystals with controllable morphology, Mater. Res. Bull. 83 (2016) 225–229, https://doi.org/10.1016/j.materresbull.2016.06.010.
[58] Y. Cheng, J. Huang, J. Li, L. Cao, Z. Xu, J. Wu, S. Cao, H. Hu, Structure-controlled synthesis and electrochemical properties of $NH_4V_3O_8$ as cathode material for Lithium ion batteries, Electrochim. Acta 212 (2016) 217–224, https://doi.org/10.1016/j.electacta.2016.07.008.
[59] T. Arul Raja, P. Vickraman, A. Simon Justin, B. Joji Reddy, Microwave Synthesis of Zinc Ammonium Phosphate/Reduced Graphene Oxide Hybrid Composite for High Energy Density Supercapacitors, Phys. Status Solidi A 217 (2020) 1900736, https://doi.org/10.1002/pssa.201900736.
[60] S. Lee, W. Cho, D. Hwang, T. Lee, Y. Kang, S. Im, Synthesis of poly(3,4-ethylene dioxythiophene)/ammonium vanadate nanofiber composites for counter electrode of dye-sensitized solar cells, Electrochim. Acta 245 (2017) 607–614, https://doi.org/10.1016/j.electacta.2017.05.194.
[61] S. Lee, C. Park, J. Park, S. Kim, S. Im, H. Ahn, Synthesis of conducting polymer-intercalated vanadate nanofiber composites using a sonochemical method for high performance pseudocapacitor applications, J. Power Sources 414 (2019) 460–469, https://doi.org/10.1016/j.jpowsour.2019.01.031.
[62] T. Kozawa, K. Fukuyama, A. Kondo, M. Naito, Wet milling synthesis of $NH_4CoPO_4{\cdot}H_2O$ platelets: Formation reaction, growth mechanism, and conversion into high-voltage $LiCoPO_4$ cathode for Li-ion batteries, Mater. Res. Bull. 135 (2021), 111149, https://doi.org/10.1016/j.materresbull.2020.111149.
[63] H. Pang, Z. Yan, W. Wang, J. Chen, J. Zhang, H. Zheng, Facile fabrication of $NH_4CoPO_4{\cdot}H_2O$ nano/microstructures and their primarily application as electrochemical supercapacitor, Nanoscale 4 (2012) 5946–5953, https://doi.org/10.1039/C2NR31208E.
[64] C. Chen, N. Zhang, Y. He, B. Liang, R. Ma, X. Liu, Controllable Fabrication of Amorphous Co—Ni Pyrophosphates for Tuning Electrochemical Performance in Supercapacitors, ACS Appl. Mater. Interfaces 8 (2016) 23114–23121, https://doi.org/10.1021/acsami.6b07640.
[65] X. Zhao, L. Mao, Q. Cheng, J. Li, F. Liao, G. Yang, L. Xie, C. Zhao, L. Chen, Two-dimensional Spinel Structured Co-based Materials for High Performance Supercapacitors: A Critical Review, Chem. Eng. J. 387 (2020), 124081, https://doi.org/10.1016/j.cej.2020.124081.
[66] Y. Jiang, L. Chen, H. Zhang, Q. Zhang, W. Chen, J. Zhu, D. Song, Two-dimensional Co_3O_4 thin sheets assembled by 3D interconnected nanoflake array framework structures with enhanced supercapacitor performance derived from coordination complexes, Chem. Eng. J. 292 (2016) 1–12, https://doi.org/10.1016/j.cej.2016.02.009.
[67] Y. Li, B. Huang, X. Zhao, Z. Luo, S. Liang, H. Qin, L. Chen, Zeolitic imidazolate framework-L-assisted synthesis of inorganic and organic anion-intercalated hetero-trimetallic layered double hydroxide sheets as advanced electrode materials for aqueous asymmetric super-capacitor battery, J. Power Sources 527 (2022), 231149, https://doi.org/10.1016/j.jpowsour.2022.231149.
[68] B. Li, Y. Shi, K. Huang, M. Zhao, J. Qiu, H. Xue, H. Pang, Cobalt-Doped Nickel Phosphite for High Performance of Electrochemical Energy Storage, Small 14 (2018) 1703811, https://doi.org/10.1002/smll.201703811.
[69] Z. Chen, D.- Xiong, X. Zhang, H. Ma, M. Xia, Y. Zhao, Construction of a novel hierarchical structured NH_4-Co-Ni phosphate toward an ultrastable aqueous hybrid capacitor, Nanoscale 8 (2016) 6636–6645, https://doi.org/10.1039/C5NR08963H.
[70] P. Wang, Y. Zhang, H. Jiang, X. Dong, C. Meng, Ammonium vanadium oxide framework with stable NH_4^+ aqueous storage for flexible quasi-solid-state supercapacitor, Chem. Eng. J. 427 (2022), 131548, https://doi.org/10.1016/j.cej.2021.131548.
[71] B. Mahmoud, A. Mirghni, K. Oyedotun, O. Fasakin, N. Manyala, Nanoplatelets ammonium nickel-cobalt phosphate graphene foam composite as novel electrode material for hybrid supercapacitors, J. Alloys Compd. 883 (2021), 160897, https://doi.org/10.1016/j.jallcom.2021.160897.
[72] S. Zhang, H. Gao, J. Zhou, Reduced graphene oxide-modified Ni-Co phosphate nanosheet self-assembled microplates as high-performance electrode materials for supercapacitors, J. Alloys Compd. 746 (2018) 549–556, https://doi.org/10.1016/j.jallcom.2018.02.008.
[73] C. Chen, N. Zhang, X. Liu, Y. He, H. Wan, B. Liang, R. Ma, A. Pan, V. Roy, Polypyrrole-Modified $NH_4NiPO_4{\cdot}H_2O$ Nanoplate Arrays on Ni Foam for Efficient Electrode in Electrochemical Capacitors, ACS Sustain. Chem. Eng. 4 (2016) 5578–5584, https://doi.org/10.1021/acssuschemeng.6b01347.
[74] X. Zhao, L. Mao, Q. Cheng, F. Liao, G. Yang, L. Chen, A new sodium vanadyl fluorophosphate as high-rate and stable cathode for aqueous hybrid sodium-zinc batteries, Chem. Commun. 58 (2022) 7522–7525, https://doi.org/10.1039/D2CC02790A.
[75] M. Sandhiya, Vivekanand, S. Suresh Balaji, M. Sathish, Unrevealed Performance of NH_4VO_3 as a Redox-Additive for Augmenting the Energy Density of a Supercapacitor, J. Phys. Chem. C 125 (15) (2021) 8068–8079.
[76] E. Cevik, A. Bozkurt, M. Hassan, M. Gondal, T. Qahtan, Redox-Mediated Poly(2-acrylamido-2-methyl-1-propanesulfonic acid)/Ammonium Molybdate Hydrogels for Highly Effective Flexible Supercapacitors, ChemElectroChem 6 (2019) 2876–2882, https://doi.org/10.1002/celc.201900490.
[77] Y. Lin, J. Li, P. Ren, X. Yang, $NH_4V_4O_{10}$ nanobelts vertically grown on 3D TiN nanotube arrays as high-performance electrode materials of supercapacitors, RSC Adv. 11 (2021) 8468–8474, https://doi.org/10.1039/D0RA09736E.
[78] F. Zhan, S. Liu, Q. He, X. Zhao, M. Han, Y. Yamauchi, L. Chen, Metal–organic framework-derived heteroatom-doped nanoarchitectures for electrochemical energy storage: recent advances and future perspectives, Energy Storage Mater. 52 (2022) 685–735, https://doi.org/10.1016/j.ensm.2022.08.035.
[79] H. Wang, K. Huang, Y. Ren, X. Huang, S. Liu, W. Wang, $NH_4V_3O_8$/carbon nanotubes composite cathode material with high capacity and good rate capability, J. Power Sources 196 (2011) 9786–9791, https://doi.org/10.1016/j.jpowsour.2011.08.015.
[80] H. Wang, Y. Ren, W. Wang, X. Huang, K. Huang, Y. Wang, S. Liu, $NH_4V_3O_8$ nanorod as a high performance cathode material for rechargeable Li-ion batteries, J. Power Sources 199 (2012) 315–321, https://doi.org/10.1016/j.jpowsour.2011.10.069.
[81] N. Wang, W. Chen, L. Mai, Y. Dai, Selected-control hydrothermal synthesis and formation mechanism of 1D ammonium vanadate, J. Solid State Chem. 181 (2008) 652–657, https://doi.org/10.1016/j.jssc.2007.12.036.
[82] K. Zhang, G. Zhang, X. Liu, Z. Su, H. Li, Large scale hydrothermal synthesis and electrochemistry of ammonium vanadium bronze nanobelts, J. Power Sources 157 (2006) 528–532, https://doi.org/10.1016/j.jpowsour.2005.07.043.
[83] H. Wang, K. Huang, C. Huang, S. Liu, Y. Ren, X. Huang, $(NH_4)_{0.5}V_2O_5$ nanobelt with good cycling stability as cathode material for Li-ion battery, J. Power Sources 196 (2011) 5645–5650, https://doi.org/10.1016/j.jpowsour.2011.02.046.
[84] S. Sarkar, P. Veluri, S. Mitra, Morphology controlled synthesis of layered $NH_4V_4O_{10}$ and the impact of binder on stable high rate electrochemical performance, Electrochim. Acta 132 (2014) 448–456, https://doi.org/10.1016/j.electacta.2014.03.144.
[85] H. Qin, S. Liang, L. Chen, Y. Li, Z. Luo, L. Chen, Recent advances in vanadium-based nanomaterials and their composites as high-performance electrode materials for supercapacitors, Sustain. Energy Fuels 4 (2020) 4902–4933, https://doi.org/10.1039/D0SE00897D.

[86] J. Heo, H. Bu, J. Hyoung, S. Hong, Ammonium Vanadium Bronze, $(NH_4)_2V_7O_{16}$, as a New Lithium Intercalation Host Material, Inorg. Chem. 59 (2020) 4320–4327, https://doi.org/10.1021/acs.inorgchem.9b03160.

[87] Y. Ma, M. Wu, X. Jin, R. Shu, C. Hu, T. Xu, J. Li, X. Meng, X. Cao, $(NH_4)_2V_7O_{16}$ Microbricks as a Novel Anode for Aqueous Lithium-Ion Battery with Good Cyclability, Chem. Eur. J. 27 (2021) 12341–12351, https://doi.org/10.1002/chem.202101431.

[88] M. Prześniak-Welenc, M. Nadolska, A. Nowak, K. Sadowska, Pressure in charge. Neglected parameter in hydrothermal synthesis turns out to be crucial for electrochemical properties of ammonium vanadates, Electrochim. Acta 339 (2020), 135919, https://doi.org/10.1016/j.electacta.2020.135919.

[89] H. Fei, Z. Shen, J. Wang, H. Zhou, D. Ding, T. Chen, Flower-like $(NH_4)_{0.83}Na_{0.43}V_4O_{10}{\cdot}0.26H_2O$ nano-structure for stable lithium battery electrodes, J. Power Sources 189 (2009) 1164–1166, https://doi.org/10.1016/j.jpowsour.2009.01.028.

[90] W. Luo, X. Hu, Y. Sun, Y. Huang, Electrospinning of carbon-coated MoO_2 nanofibers with enhanced lithium-storage properties, Phys. Chem. Chem. Phys. 13 (2011) 16735–16740, https://doi.org/10.1039/C1CP22184A.

[91] W. Wu, Y. Fan, X. Wu, S. Liao, S. Li, Preparation via solid-state reaction at room temperature and characterization of layered nanocrystalline $NH_4MnPO_4{\cdot}H_2O$, J. Phys. Chem. Solids 70 (2009) 584–587, https://doi.org/10.1016/j.jpcs.2008.12.016.

[92] X. Zhao, L. Mao, Q. Cheng, F. Liao, G. Yang, L. Chen, Dual-cation Preintercalated and Amorphous Carbon Confined Vanadium Oxides as a Superior Cathode for Aqueous Zinc-ion Batteries, Carbon 186 (2022) 160–170, https://doi.org/10.1016/j.carbon.2021.10.013.

[93] J. Lai, H. Tang, X. Zhu, Y. Wang, A hydrated $NH_4V_3O_8$ nanobelt electrode for superior aqueous and quasi-solid-state zinc ion batteries, J. Mater. Chem. A 7 (2019) 23140–23148, https://doi.org/10.1039/C9TA07822C.

[94] X. Zhao, L. Mao, Q. Cheng, F. Liao, G. Yang, L. Chen, A new sodium ion preintercalated and oxygen vacancy-enriched vanadyl phosphate cathode for aqueous zinc-ion batteries, J. Colloid Interf. Sci. 627 (2022) 1021–1029, https://doi.org/10.1016/j.jcis.2022.07.119.

[95] H. Jiang, Y. Zhang, Z. Pan, L. Xu, J. Zheng, Z. Gao, T. Hu, C. Meng, Facile hydrothermal synthesis and electrochemical properties of $(NH_4)_2V_{10}O_{25}{\cdot}8H_2O$ nanobelts for high-performance aqueous zinc ion batteries, Electrochim. Acta 332 (2020), 135506, https://doi.org/10.1016/j.electacta.2019.135506.

[96] F. Wan, Z. Niu, Design Strategies for Vanadium-based Aqueous Zinc-Ion Batteries, Angew. Chem. Int. Ed. 58 (2019) 16358–16367, https://doi.org/10.1002/anie.201903941.

[97] N. Zhang, F. Cheng, J. Liu, L. Wang, X. Long, X. Liu, F. Li, J. Chen, Rechargeable aqueous zinc-manganese dioxide batteries with high energy and power densities, Nat. Commun. 8 (2017) 405, https://doi.org/10.1038/s41467-017-00467-x.

[98] Z. Liu, G. Pulletikurthi, F. Endres, A Prussian Blue/Zinc Secondary Battery with a Bio-Ionic Liquid-Water Mixture as Electrolyte, ACS Appl. Mater. Interfaces 8 (2016) 12158–12164, https://doi.org/10.1021/acsami.6b01592.

[99] G. Zakharova, C. Täschner, T. Kolb, C. Jähne, A. Leonhardt, B. Büchner, R. Klingeler, Morphology controlled $NH_4V_3O_8$ microcrystals by hydrothermal synthesis, Dalton Trans. 42 (2013) 4897–4902, https://doi.org/10.1039/C3DT32550D.

[100] L. Xu, Y. Zhang, H. Jiang, J. Zheng, X. Dong, T. Hu, C. Meng, Facile hydrothermal synthesis and electrochemical properties of $(NH_4)_2V_6O_{16}$ nanobelts for aqueous rechargeable zinc ion batteries, Colloids Surf. A Physicochem. Eng. Asp. 593 (2020), 124621, https://doi.org/10.1016/j.colsurfa.2020.124621.

[101] N. Qiu, H. Chen, Z. Yang, Y. Zhu, W. Liu, Y. Wang, Porous hydrated ammonium vanadate as a novel cathode for aqueous rechargeable Zn-ion batteries, Chem. Commun. 56 (2020) 3785–3788, https://doi.org/10.1039/C9CC09914J.

[102] L. Xu, Y. Zhang, J. Zheng, H. Jiang, T. Hu, C. Meng, Ammonium ion intercalated hydrated vanadium pentoxide for advanced aqueous rechargeable Zn-ion batteries, Mater. Today Energy 18 (2020), 100509, https://doi.org/10.1016/j.mtener.2020.100509.

[103] G. Yang, T. Wei, C. Wang, Self-Healing Lamellar Structure Boosts Highly Stable Zinc-Storage Property of Bilayered Vanadium Oxides, ACS Appl. Mater. Interfaces 10 (2018) 35079–35089, https://doi.org/10.1021/acsami.8b10849.

[104] Q. Zong, W. Du, C. Liu, H. Yang, Q. Zhang, Z. Zhou, M. Atif, M. Alsalhi, G. Cao, Enhanced Reversible Zinc Ion Intercalation in Deficient Ammonium Vanadate for High-Performance Aqueous Zinc-Ion Battery, Nano-Micro Lett. 13 (2021) 116, https://doi.org/10.1007/s40820-021-00641-3.

[105] Q. Li, X. Rui, D. Chen, Y. Feng, N. Xiao, L. Gan, Q. Zhang, Y. Yu, S. Huang, A High-Capacity Ammonium Vanadate Cathode for Zinc-Ion Battery, Nano-Micro Lett. 12 (2020) 67, https://doi.org/10.1007/s40820-020-0401-y.

[106] T. Zhu, B. Mai, P. Hu, Z. Liu, C. Cai, X. Wang, L. Zhou, Ammonium Ion and Structural Water Co-Assisted Zn^{2+} Intercalation/De-Intercalation in $NH_4V_4O_{10}{\bullet}0.28H_2O$, Chin. J. Chem. 39 (2021) 1885–1890, https://doi.org/10.1002/cjoc.202100004.

[107] R. Sun, Z. Qin, X. Liu, C. Wang, S. Lu, Y. Zhang, H. Fan, Intercalation Mechanism of the Ammonium Vanadate $(NH_4V_4O_{10})$ 3D Decussate Superstructure as the Cathode for High-Performance Aqueous Zinc-Ion Batteries, ACS Sustain. Chem. Eng. 9 (2021) 11769–11777, https://doi.org/10.1021/acssuschemeng.1c03101.

[108] T. Wei, Q. Li, G. Yang, C. Wang, Highly reversible and long-life cycling aqueous zinc-ion battery based on ultrathin $(NH_4)_2V_{10}O_{25}{\cdot}8H_2O$ nanobelts, J. Mater. Chem. A 6 (2018) 20402–20410, https://doi.org/10.1039/C8TA06626D.

[109] F. Cui, F. Hu, X. Yu, C. Guan, G. Song, K. Zhu, In-situ tuning the NH_4^+ extraction in $(NH_4)_2V_4O_9$ nanosheets towards high performance aqueous zinc ion batteries, J. Power Sources 492 (2021), 229629, https://doi.org/10.1016/j.jpowsour.2021.229629.

[110] Y. Chen, J. Zhao, Y. Wang, Quasi-Solid-State Zinc Ion Rechargeable Batteries for Subzero Temperature Applications, ACS Appl. Energy Mater. 3 (2020) 9058–9065, https://doi.org/10.1021/acsaem.0c01452.

[111] H. Jiang, Y. Zhang, Y. Liu, J. Yang, L. Xu, P. Wang, Z. Gao, J. Zheng, C. Meng, Z. Pan, In situ grown 2D hydrated ammonium vanadate nanosheets on carbon cloth as a free-standing cathode for high-performance rechargeable Zn-ion batteries, J. Mater. Chem. A 8 (2020) 15130–15139, https://doi.org/10.1039/D0TA05065B.

[112] H. Jiang, Y. Zhang, L. Xu, Z. Gao, J. Zheng, Q. Wang, C. Meng, J. Wang, Fabrication of $(NH_4)_2V_3O_8$ nanoparticles encapsulated in amorphous carbon for high capacity electrodes in aqueous zinc ion batteries, Chem. Eng. J. 382 (2020), 122844, https://doi.org/10.1016/j.cej.2019.122844.

[113] M. Tamilselvan, T. Sreekanth, K. Yoo, J. Kim, Ultrathin ammonium vanadate nanoflakes on carbon fiber – A binder-free high-rate capability cathode for aqueous medium zinc ion storage, J. Alloys Compd. 876 (2021), 160130, https://doi.org/10.1016/j.jallcom.2021.160130.

[114] P. He, S. Chen, Cathode strategies to improve the performance of zinc-ion batteries, Electrochem. Sci. Adv. 2 (2022) e2100090.

[115] Y. Zhang, L. Tao, C. Xie, D. Wang, Y. Zou, R. Chen, Y. Wang, C. Jia, S. Wang, Defect Engineering on Electrode Materials for Rechargeable Batteries, Adv. Mater. 32 (2020) 1905923, https://doi.org/10.1002/adma.201905923.

[116] F. Cui, D. Wang, F. Hu, X. Yu, C. Guan, G. Song, F. Xu, K. Zhu, Deficiency and surface engineering boosting electronic and ionic kinetics in $NH_4V_4O_{10}$ for high-performance aqueous zinc-ion battery, Energy Stor. Mater. 44 (2022) 197–205, https://doi.org/10.1016/j.ensm.2021.10.001.

[117] J. Li, N. Luo, F. Wan, S. Zhao, Z. Li, W. Li, J. Guo, P. Shearing, D. Brett, C. Carmalt, G. Chai, G. He, I. Parkin, Defected vanadium bronzes as superb cathodes in aqueous zinc-ion batteries, Nanoscale 12 (2020) 20638–20648, https://doi.org/10.1039/D0NR03394D.

[118] T. He, Y. Ye, H. Li, S. Weng, Q. Zhang, M. Li, T. Liu, J. Cheng, X. Wang, J. Lu, B. Wang, Oxygen-deficient ammonium vanadate for flexible aqueous zinc batteries with high energy density and rate capability at −30 °C, Mater. Today 43 (2021) 53–61, https://doi.org/10.1016/j.mattod.2020.11.019.

[119] Y. Bai, H. Zhang, Q. Hu, Y. Zhou, B. Xiang, Tuning the kinetics of binder-free ammonium vanadate cathode via defect modulation for ultrastable rechargeable zinc ion batteries, Nano Energy 90 (2021), 106596, https://doi.org/10.1016/j.nanoen.2021.106596.

[120] Y. Lu, L. Liu, D. Mandler, P. Lee, High switching speed and coloration efficiency of titanium-doped vanadium oxide thin film electrochromic devices, J. Mater. Chem. C 1 (2013) 7380–7386, https://doi.org/10.1039/C3TC31508H.

[121] X. Wang, L. Ye, Y. Zou, L. Zhao, Q. Jiang, Constructing ultra-long life and super-rate rechargeable aqueous zinc-ion batteries by integrating Mn doped V_6O_{13} nanoribbons with sulfur-nitrogen modified porous carbon, Mater. Today Energy 19 (2021), 100593, https://doi.org/10.1016/j.mtener.2020.100593.

[122] X. Wang, A. Naveed, T. Zeng, T. Wan, H. Zhang, Y. Zhou, A. Dou, M. Su, Y. Liu, D. Chu, Sodium ion stabilized ammonium vanadate as a high-performance aqueous zinc-ion battery cathode, Chem. Eng. J. 446 (2022), 137090, https://doi.org/10.1016/j.cej.2022.137090.

[123] D. Muthuraj, A. Sarkar, M. Panda, M. Adil, A. Sagdeo, S. Mitra, Zirconium-Doped Vanadium Oxide and Ammonium Linked Layered Cathode to Construct a Full-Cell Magnesium-Ion Battery: A Realization and Structural, Electrochemical Study, Batteries Supercaps 4 (2021) 1757–1770, https://doi.org/10.1002/batt.202100149.

[124] G. Qu, J. Wang, G. Liu, B. Tian, C. Su, Z. Chen, J. Rueff, Z. Wang, Vanadium Doping Enhanced Electrochemical Performance of Molybdenum Oxide in Lithium-Ion Batteries, Adv. Funct. Mater. 29 (2019) 1805227, https://doi.org/10.1002/adfm.201805227.

[125] H. Wang, R. Jing, J. Shi, M. Zhang, S. Jin, Z. Xiong, L. Guo, Q. Wang, Mo-doped $NH_4V_4O_{10}$ with enhanced electrochemical performance in aqueous Zn-ion batteries, J. Alloys Compd. 858 (2021), 158380, https://doi.org/10.1016/j.jallcom.2020.158380.

[126] S. Chen, Y. Zhang, H. Geng, Y. Yang, X. Rui, C. Li, Zinc ions pillared vanadate cathodes by chemical pre-intercalation towards long cycling life and low-temperature zinc ion batteries, J. Power Sources 441 (2019), 227192, https://doi.org/10.1016/j.jpowsour.2019.227192.

[127] R. Sun, S. Dong, F. Xu, Z. Li, C. Wang, S. Lu, H. Fan, Co-intercalation strategy of constructing partial cation substitution of ammonium vanadate (NH4)2V6O16 for stable zinc ion storage, Dalton Trans. 51 (2022) 7607–7612, https://doi.org/10.1039/D2DT00665K.

[128] M. Tamilselvan, T. Sreekanth, K. Yoo, J. Kim, Wide interlayer spacing ammonium vanadate $(NH_4)_{0.37}V_2O_5{\cdot}0.15(H_2O)$ cathode for rechargeable aqueous zinc-ion batteries, J. Ind. Eng. Chem. 93 (2021) 176–185, https://doi.org/10.1016/j.jiec.2020.09.021.

[129] H. Jiang, Y. Zhang, Z. Pan, L. Xu, J. Zheng, Z. Gao, T. Hu, C. Meng, J. Wang, $NH_4V_3O_8{\cdot}0.5H_2O$ nanobelts with intercalated water molecules as a high performance zinc ion battery cathode, Mater. Chem. Front. 4 (2020) 1434–1443, https://doi.org/10.1039/D0QM00051E.

[130] D. Bin, W. Huo, Y. Yuan, J. Huang, Y. Liu, Y. Zhang, F. Dong, Y. Wang, Y. Xia, Organic-Inorganic-Induced Polymer Intercalation into Layered Composites for Aqueous Zinc-Ion Battery, Chem 6 (2020) 968–984, https://doi.org/10.1016/j.chempr.2020.02.001.

[131] J. Ming, J. Guo, C. Xia, W. Wang, H. Alshareef, Zinc-ion batteries: Materials, mechanisms, and applications, Mater. Sci. Eng. R Rep. 135 (2019) 58–84, https://doi.org/10.1016/j.mser.2018.10.002.

[132] J. Zhang, M. Wang, M. Zeng, X. Li, L. Chen, Z. Yang, J. Chen, B. Guo, Z. Ma, X. Li, Sulfite modified and ammonium ion intercalated vanadium hydrate with

enhanced redox kinetics for aqueous zinc ion batteries, J. Power Sources 496 (2021), 229832, https://doi.org/10.1016/j.jpowsour.2021.229832.
[133] W. Deng, Y. Xu, X. Zhang, C. Li, Y. Liu, K. Xiang, H. Chen, $(NH_4)_2Co_2V_{10}O_{28}\cdot16H_2O/(NH_4)_2V_{10}O_{25}\cdot8H_2O$ heterostructure as cathode for high-performance aqueous Zn-ion batteries, J. Alloys Compd. 903 (2022), 163824, https://doi.org/10.1016/j.jallcom.2022.163824.
[134] C. Huang, S. Liu, J. Feng, Y. Wang, Q. Fan, Q. Kuang, Y. Dong, Y. Zhao, Optimizing engineering of rechargeable aqueous zinc ion batteries to enhance the zinc ions storage properties of cathode material, J. Power Sources 490 (2021), 229528, https://doi.org/10.1016/j.jpowsour.2021.229528.
[135] H. Fei, X. Liu, Y. Lin, M. Wei, Facile synthesis of ammonium vanadium oxide nanorods for Na-ion battery cathodes, J. Colloid Interface Sci. 428 (2014) 73–77, https://doi.org/10.1016/j.jcis.2014.04.029.
[136] Y. Xu, H. Dong, M. Zhou, C. Zhang, Y. Wu, W. Li, Y. Dong, Y. Lei, Ammonium Vanadium Bronze as a Potassium-Ion Battery Cathode with High Rate Capability and Cyclability, Small Methods 3 (2019) 1800349, https://doi.org/10.1002/smtd.201800349.
[137] T. Vo, H. Kim, J. Hur, W. Choi, I. Kim, Surfactant-assisted ammonium vanadium oxide as a superior cathode for calcium-ion batteries, J. Mater. Chem. A 6 (2018) 22645–22654, https://doi.org/10.1039/C8TA07831A.
[138] H. Li, J. Yang, J. Cheng, T. He, B. Wang, Flexible aqueous ammonium-ion full cell with high rate capability and long cycle life, Nano Energy 68 (2020), 104369, https://doi.org/10.1016/j.nanoen.2019.104369.
[139] L. Yao, P. Zou, L. Su, Y. Wu, Y. Pan, R. Fu, H. Min, L. Zhong, H. Xin, L. Sun, F. Xu, In-situ TEM revisiting $NH_4V_4O_{10}$ to unveil the unknown sodium storage mechanism as an anode material, Nano Energy 87 (2021), 106182, https://doi.org/10.1016/j.nanoen.2021.106182.
[140] H. Fei, X. Liu, H. Li, M. Wei, Enhanced electrochemical performance of ammonium vanadium bronze through sodium cation intercalation and optimization of electrolyte, J. Colloid Interface Sci. 418 (2014) 273–276, https://doi.org/10.1016/j.jcis.2013.12.022.
[141] N. Yabuuchi, K. Kubota, M. Dahbi, S. Komaba, Research Development on Sodium-Ion Batteries, Chem. Rev. 114 (2014) 11636–11682, https://doi.org/10.1021/cr500192f.
[142] A. Sarkar, S. Sarkar, T. Sarkar, P. Kumar, M. Bharadwaj, S. Mitra, Rechargeable Sodium-Ion Battery: High-Capacity Ammonium Vanadate Cathode with Enhanced Stability at High Rate, ACS Appl. Mater. Interfaces 7 (2015) 17044–17053, https://doi.org/10.1021/acsami.5b03210.
[143] X. Liu, Z. Li, H. Fei, M. Wei, Composite of K-doped $(NH_4)_2V_3O_8$/graphene as an anode material for sodium-ion batteries, Dalton Trans. 44 (2015) 18864–18869, https://doi.org/10.1039/C5DT03239C.
[144] E. Esparcia, M. Chae, J. Ocon, S. Hong, Ammonium Vanadium Bronze ($NH_4V_4O_{10}$) as a High-Capacity Cathode Material for Nonaqueous Magnesium-Ion Batteries, Chem. Mater. 30 (11) (2018) 3690–3696.
[145] L. Wei, R. Lian, D. Wang, Y. Zhao, D. Yang, H. Zhao, Y. Wang, G. Chen, Y. Wei, Magnesium Ion Storage Properties in a Layered $(NH_4)_2V_6O_{16}\cdot1.5H_2O$ Nanobelt Cathode Material Activated by Lattice Water, ACS Appl. Mater. Interfaces 13 (2021) 30625–30632, https://doi.org/10.1021/acsami.1c06398.
[146] H. Kim, J. Kim, M. Bianchini, D. Seo, J. Rodriguez-Garcia, G. Ceder, Recent Progress and Perspective in Electrode Materials for K-Ion Batteries, Adv. Energy Mater. 8 (2018) 1702384, https://doi.org/10.1002/aenm.201702384.
[147] Y. Fan, Z. Qu, W. Zhong, Z. Hu, H. Younus, C. Yang, X. Wang, S. Zhang, Understanding the Effect of Interplanar Space and Preintercalated Cations of Vanadate Cathode Materials on Potassium-Ion Battery Performance, ACS Appl. Mater. Interfaces 13 (2021) 7377–7388, https://doi.org/10.1021/acsami.0c23152.
[148] J. Han, A. Varzi, S. Passerini, The Emergence of Aqueous Ammonium-Ion Batteries, Angew. Chem. Int. Ed. 61 (2022) e202115046.
[149] R. Zhang, S. Wang, S. Chou, H. Jin, Research Development on Aqueous Ammonium-Ion Batteries, Adv. Funct. Mater. 32 (2022) 2112179, https://doi.org/10.1002/adfm.202112179.
[150] S. Farai Kuchena, Y. Wang, A Full Flexible NH_4^+ Ion Battery Based on the Concentrated Hydrogel Electrolyte for Enhanced Performance, Chem. Eur. J. 27 (2021) 15450–15459, https://doi.org/10.1002/chem.202102442.
[151] J. Yang, S. Muhammad, M. Jo, H. Kim, K. Song, D. Agyeman, Y. Kim, W. Yoon, Y. Kang, In situ analyses for ion storage materials, Chem. Soc. Rev. 45 (2016) 5717–5770, https://doi.org/10.1039/C5CS00734H.
[152] D. Bin, Y. Liu, B. Yang, J. Huang, X. Dong, X. Zhang, Y. Wang, Y. Xia, Engineering a High-Energy-Density and Long Lifespan Aqueous Zinc Battery via Ammonium Vanadium Bronze, ACS Appl. Mater. Interfaces 11 (2019) 20796–20803, https://doi.org/10.1021/acsami.9b03159.
[153] T. Sarkar, P. Kumar, M. Bharadwaj, U. Waghmare, Structural transformation during Li/Na insertion and theoretical cyclic voltammetry of the δ-$NH_4V_4O_{10}$ electrode: a first-principles study, Phys. Chem. Chem. Phys. 18 (2016) 9344–9348, https://doi.org/10.1039/C5CP07782F.